Rare-gas electron-energy spectra produced by collision-free multiquantum processes

U. Johann, T. S. Luk, H. Egger,* and C. K. Rhodes
Department of Physics, University of Illinois at Chicago, P.O. Box 4348, Chicago, Illinois 60680
(Received 8 November 1985)

The energy spectra of electrons generated by collision-free multiphoton ionization of Xe, Kr, Ar, Ne, and He irradiated at intensities up to $\sim 10^{15}$ W/cm^2 with picosecond 193-nm (6.41-eV) radiation have been studied with an energy resolution of ~ 50 meV. The formation of multiply charged ions by a sequential process of ionization has been directly detected in the electron spectra by the observation of a characteristic pattern of interwoven above-threshold-ionization ladder line series. The appearance and relative intensity of specific electron lines depends strongly on the presence of near-resonances and features of the interaction involving the laser pulse shape, saturation, and the shift of the ionization threshold arising from the influence of the ponderomotive potential. The experimental results are compared qualitatively with data from ion time-of-flight experiments and with differing models of multiphoton ionization.

I. INTRODUCTION

With the development of spectrally bright infrared and ultraviolet light sources in the last decade, it has become possible to study the detailed mechanism of nonlinear coupling of an intense laser field to isolated atoms unaffected by collisions. Several experiments[1] have been performed to analyze the ion charge-state production,[2–5] to determine the electron-energy spectrum,[6–9] and to measure the optical radiation emitted.[4,10] For processes that occur under these conditions, one of the areas of substantial interest involves the possibility of producing atomic excitations suitable for the generation of stimulated emission in the x-ray range.[1(b)]

For a "weak" laser field (intensity $< 10^{11}$ W/cm^2), the coupling of radiation to an isolated atom can be described fairly well within the framework of lowest-order perturbation theory (LOPT) in which only one electron at a time is assumed to be involved in multiphoton ionization.[1,11] However, for much higher laser intensities (10^{12}–10^{17} W/cm^2), the situation is poorly understood and other coupling mechanisms involving many electrons may play an appreciable role.

Experimentally, the electron-energy spectra produced by radiation with a quantum energy $\hbar\omega$ exhibit certain salient characteristics. A prominent feature of the observed electron spectra is the process known as above-threshold ionization (ATI), a phenomenon associated with the absorption of a number of photons N greater than the minimum value $N_{\min}$ required, on energetic grounds, to produce ionization.[7,12] When $N > N_{\min}$, the measured electron-energy spectrum consists of a series of discrete lines each corresponding to the order N with an energy separation of adjacent orders equaling the quantum $\hbar\omega$. Furthermore, it is found that the electron lines are not significantly shifted by the effect of the ponderomotive force.[13] Recently, two-photon free-free transitions have also been analyzed.[14] In addition, the order of nonlinearity observed for higher-order ATI electron lines is approximately the same as for the threshold ionization line, a finding which stands in contradiction to LOPT.[13] This result is, however, consistent with the order of nonlinearity measured in ion-yield experiments,[15] although more recent experiments may alter this picture.[16] It is also seen that certain low-energy electron lines disappear with increasing laser intensity at characteristic values which depend upon the frequency of irradiation.[13] Finally, high-energy electrons (> 100 eV) have been observed[8,17] in low-resolution experiments with intense infrared lasers ($> 10^{15}$ W/cm^2).

Studies[2,3,4] of ion production by multiquantum processes have indicated the presence of an anomalously strong coupling for materials in certain regions of the periodic table. It appeared that the magnitude of this coupling is sufficiently great that reasonable account cannot be made by a mechanism involving the sequential stripping of individual valence electrons in a stepwise process. Furthermore, the results on ion production exhibited readily observed dependences on the atomic shell structure, or equivalently, the atomic number, and the frequency of irradiation.

The hypothesis has been advanced that multiply excited states representing highly organized coherent motions of several valence-shell electrons may play an important role in the coupling at sufficiently high laser intensity.[18] This mechanism is an alternative to the sequential process described above if the multiply excited state is produced by a direct multiphoton amplitude from the neutral atomic ground state. Such an excited state would be expected to decay by multiple-electron emission to energetically available continuum states. In addition, it has been shown theoretically that multiply excited states of outer-shell electrons can transfer energy into inner-shell excitations.[19,20]

In this paper, we describe the results of experiments in which the energy spectra of electrons generated by collision-free multiphoton ionization of xenon, krypton, argon, neon, and helium irradiated at 193 nm in the intensity range spanning 10^{13}–10^{15} W/cm^2 were studied. The field strengths $|\mathbf{E}_0|$ corresponding to this range are

$0.017 \leq |\mathbf{E}_0| \leq 0.169$, as measured in atomic units (e/a_0^2). This investigation had two goals. One involved obtaining information concerning the mechanism of coupling leading to the high ion charge states observed in earlier experiments[3,4] under similar conditions, while the second sought an understanding of the conditions necessary for the production of inner-shell excitations by processes of intra-atomic energy transfer.

II. EXPERIMENTAL

A. 193-nm laser system and beam properties

For irradiation of the target gas, a 193-nm picosecond ArF* excimer laser system has been used.[21] This system delivers, in both temporal and spatial characteristics, a nearly-transform-limited output beam whose properties are the following: pulse energy ~ 40 mJ, pulse length ~ 5 ps, quantum energy $\hbar\omega \sim 6.41$ eV, and repetition rate ~ 1 Hz. In order to perform the experiments, the 193-nm beam was focused with a quartz lens ($f=205$ mm at 193 nm) into the interaction region of an electron spectrometer. As shown below, the focal volume is several times larger than the diffraction-limited value, a fact mainly attributed to imperfections in the optical system such as spherical abberation. It follows that the maximum intensity produced in the interaction region is on the order of 10^{15} W/cm^2. In addition to the short picosecond pulse, amplified spontaneous emission (ASE) at $\lambda \sim 193$ nm is also present and may represent a substantial contribution to the energy in the form of a ~ 10 ns background pulse.[21] With no picosecond input into the 193-nm amplifier chain, the ~ 10-ns ASE pulse has an energy of ~ 50—100 mJ. Although this relatively low-intensity radiation produces no detectable ionization of He, Ne, and Ar, the intensity is sufficient to singly ionize a considerable fraction of the experimental material in the focal volume for Kr and Xe. However, examination of the distributions of the pulse energies for both the ASE and picosecond components showed that the ASE focus only partially overlaps the focal volume associated with the picosecond pulse. Consequently, the ASE is expected to have little influence on the interaction dynamics of the picosecond pulse with the atoms in the focal region of the short-pulse beam. This was confirmed experimentally by changing the temporal position of the picosecond feature within the much broader ASE pulse, a procedure which, in some cases, altered only slightly the relative intensity of the electron lines. Importantly, no qualitative influence on the electron spectra was present. Finally, from analyses of the 193-nm beam,[21] it is believed that the presence in the interaction volume of large spatial and temporal spikes was unlikely.

B. Electron spectrometer and signal processing

The space charge produced in the experimental volume can appreciably alter the characteristics of the observed electron-energy spectra. In order to minimize the influence of the space charge on the electron spectra, it is necessary to substantially limit the number of electrons produced per laser pulse in the focal region. Therefore, the electron spectrometer should have a high collection efficiency in addition to a reasonable energy resolution. The magnetic mirror time-of-flight electron spectrometer designed for this purpose allows a collection solid angle of about 2π steradians at an energy resolution of approximately 50 meV. The principles of operation and physical properties of this type of spectrometer[22,23] have been extensively studied by Kruit and Read.[24]

The interaction volume, in which the electrons are produced, is located in the strong-field region (~ 3000 G) of a Co-Sm permanent magnet as shown in Fig. 1. The electrons produced are immediately bound to the magnetic field and execute a cyclotron motion as they are accelerated in the magnetic field gradient along the symmetry axis of the spectrometer. The electronic trajectories, although complicated in detail, occur with conservation of the total kinetic energy of the electrons. The laser polarization is oriented parallel to the magnetic field axis. Those electrons emitted into the forward 2π-sr solid angle enter the low-field region (1—5 G) after traveling a distance of about 200 mm with their velocity oriented nearly parallel to the z axis. The electron energy can now be measured with a time-of-flight technique. In the 800-mm drift-tube region, which is shielded against stray magnetic fields by μ-metal layers to a value less than ~ 10 mG, a weak magnetic guide field of typically 0.5—5 G is maintained by a solenoid. The time that the electrons spend in the drift tube can be increased by the application of a retarding electric field, which considerably improves the energy resolution for the more energetic electrons. The electrons are detected by a two-stage multichannel plate detector (MCP), which is connected to a transient digitizer (Tektronix 7912 AD). The data taking, processing, and storage were handled by a Digital Equipment Corporation PDP-11 computer.

Without retardation, the total flight time T for an electron from the focal volume at position Z_0 on the z axis to the detector located at point Z_D is given by

$$T(\varepsilon_0,\theta_0)=\left[\frac{m}{2\varepsilon_0}\right]^{1/2}\int_{Z_0}^{Z_D}\frac{dz}{\left[1-\frac{B(z)}{B_0}\sin^2\theta_0\right]^{1/2}}. \tag{1}$$

In expression (1) ε_0 is the initial electron kinetic energy, $0 \leq \theta_0 \leq \pi/2$ is the angular range of emission with respect to the z axis, $B(z)$ is the magnetic field as a function of position along the z axis, and $B_0 \equiv B(Z_0)$. The time distribution function dn_e/dt, for n_0 monoenergetic simultaneously generated and isotropically emitted electrons, which describes their arrival at the detector, is given by

$$\frac{dn_e}{dt}(n_0,T(\varepsilon_0,\theta_0)) = \left[\frac{\varepsilon_0}{2m}\right]^{1/2}\frac{n_0 B_0}{\cos\theta_0} \times\left[\int_{Z_0}^{Z_D}\frac{B(z)dz}{\left[1-\frac{B(z)}{B_0}\sin^2\theta_0\right]^{3/2}}\right]^{-1}. \tag{2}$$

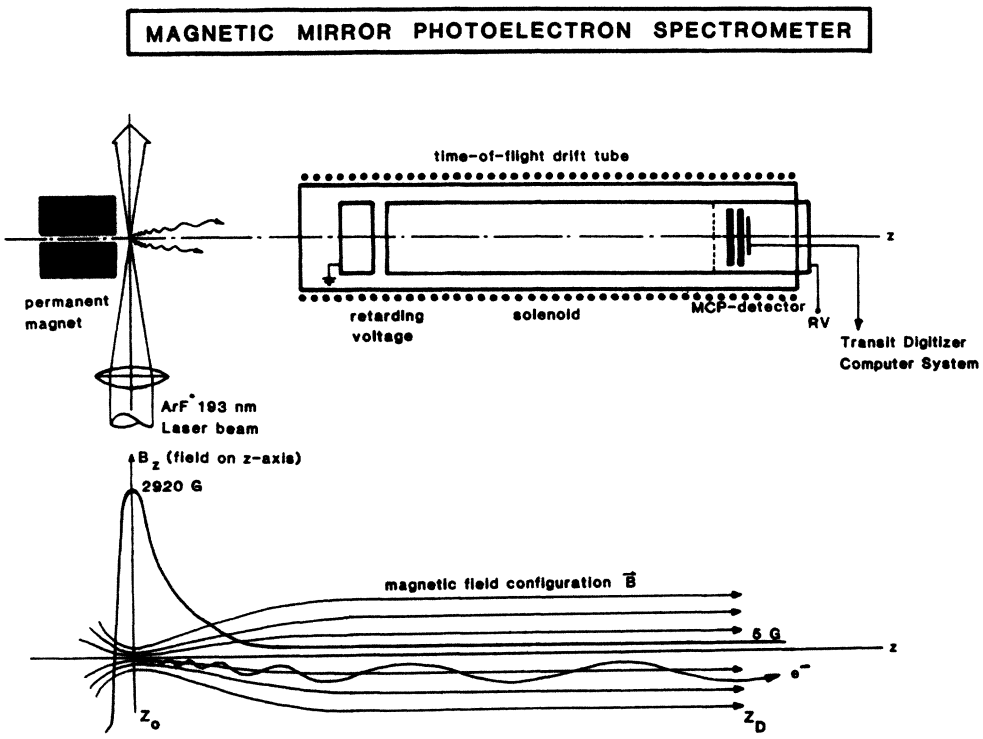

FIG. 1. Schematic diagram of the electron time-of-flight spectrometer. Also shown are the z dependence of the magnetic field on the z axis and the magnetic field configuration with a helical path of an electron moving from the high-field interaction region to the low-field region at the detector.

Physically, the spread in electron arrival times occurring at the detector arises from the influence of the magnetic field as the velocities of the electrons become parallel. For anisotropic electron emission with a $\cos^2\theta_0$ distribution,[24] Eq. (2) is multiplied by a factor of $3\cos^2\theta_0$. Fig. 2 illustrates the calculated time-of-flight distribution at the detector for anisotropic emission along with the measured influence of the retarding potential on the electron linewidth.

The target gas uniformly fills the whole vacuum system and typical operating pressures were between 2×10^{-8} and 5×10^{-6} Torr. Experimentally it was found that, depending on the laser intensity and the ionization probability, both the effects of space charge in the focal region and detector saturation could severely limit the highest useful gas density. The space charge tends to broaden the width of the electron lines, as shown in Fig. 2, and generates a low-energy tail on the distribution. Consequently, the total ion production was usually kept below ~1000 per laser pulse. At such a low signal intensity, the MCP was operated in an event-counting mode, a procedure which supresses electrical noise and allows integration over several hundred laser shots. Since the background pressure in the vacuum system was less than 10^{-8} Torr, little interference in the measured spectra was caused from electrons produced in this material.

However, since the single-photon energy of 6.41 eV is higher than any material work function, scattered laser radiation can copiously generate photoelectrons on all surfaces, especially on the magnet facing the interaction region which is located at a 6 mm distance from the focal volume. Despite careful shielding, these electrons cause an energy upshift of all electron lines by an amount ranging between ~0 and 0.8 eV, the exact value depending on the laser energy. In addition, a continuous distribution of low-energy electrons was detected which forms a background decreasing in magnitude from about ~0 to 2 eV.

Calibration of the electron energy was performed by directing a small fraction of the laser beam directly onto the MCP detector or by simply using the prompt signal generated by scattered photons hitting the detector and so providing the zero-time reference signal. The scale of the energy axis is then obtained by the identification in the spectrum of the ATI ladder lines which are separated by $\hbar\omega=6.41$ eV. This calibration can be checked by shifting the electron lines with the retarding voltage. Close to the threshold of detection, at low laser intensity, low scattered-light level, and low gas pressure, the leading edges of the asymmetric electron lines coincided to within 20 meV of their corresponding calculated positions. Contact potentials have been avoided by covering all surfaces with a layer of graphite (Aerodag G).

Information about the flatness of the spectrometer transmission, at least in the operating range for these experiments (between 0.3 and ~40 eV), can be drawn from two observations. When the drift-tube magnetic field was increased over a certain value (1—2 G), the relative electron line intensities did not change, an indication of the adiabaticity[24] of the magnetic field configurations under these conditions. Furthermore, a metal tip was installed

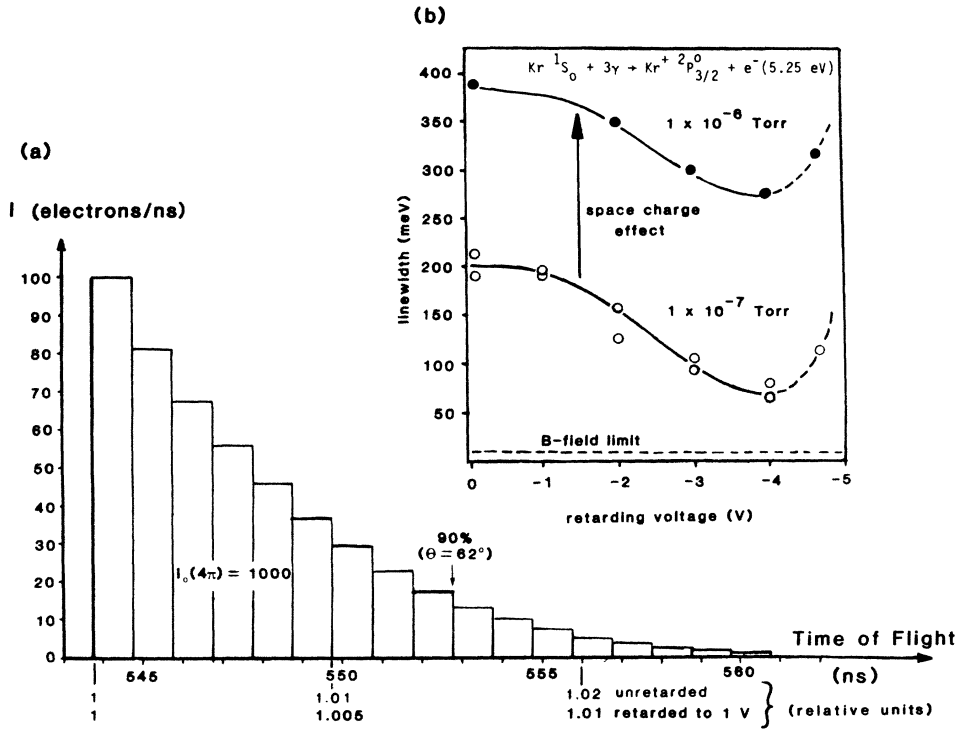

FIG. 2. (a) Calculated form of the time-of-flight electron distribution for monoenergetic electrons. An anisotropic $\cos^2\theta_0$ distribution for the emission angle θ_0 relative to the z axis is assumed. For 10-eV electrons, 90% arrive at the detector with a time difference of $\Delta T/T = 1.8\%$ corresponding to $\Delta E = 380$ meV. Retarded to 1 eV in the drift tube, the figures are $\Delta T/T = 0.8\%$ and $\Delta E \approx 17$ meV. (b) Measured linewidth of the three-photon absorption line (5.24 eV) in Kr at an intensity of $\sim 5 \times 10^{11}$ W/cm^2, leaving the ion in the $^2P^o_{3/2}$ ground state. The dependence on the retarding voltage and gas pressure is shown. The change in energy resolution and the influence of space-charge effects are evident.

near the interaction region and used to establish a static electric field to accelerate photoelectrons. Although a relatively crude test, the electron yield remained nearly constant within a factor of about 3 up to ~ 1 keV and a drift-tube magnetic field below 9 G. Depending on gas pressure, very slow electrons can be trapped in the focal region.[25] Therefore, a decrease in the sensitivity of detection is expected to exist below ~ 300 meV at a density of $\sim 10^{-6}$ Torr.

Since the magnetic field diverges in the drift region, this type of electron spectrometer exhibits a magnification whose value depends upon the ratio of the magnetic field strength in the interaction region to that present at the detector. By varying the magnetic field in the drift tube, a circle with a diameter between ~ 250 and 500 μm can be imaged onto the detector surface. With this knowledge, an approximate estimate of the interaction volume has been made through a comparison of the electron yield with the number density of the target gas. Working at a sufficiently high intensity so that the ionization of the sample is saturated, and taking into account the overall efficiency of detection, ($\sim 25\%$), determined mainly by the angle of acceptance and the channel plate sensitivity ($\sim 50\%$), we find a diameter of approximately 18 μm. This result is in good agreement with the value of ~ 14 μm estimated independently from the limit imposed by spherical abberation. Furthermore, the spectra are observed to be insensitive to the position of the focusing lens when it is moved along the laser-beam axis for a distance of about 1 mm. This indicates that the intensity varies rather slowly in the vicinity of the focal plane. Since exact information on the intensity distribution throughout the interaction volume is not known, an uncertainty of approximately a factor of 3 remains for the absolute laser intensity used in these experiments.

III. RESULTS AND DISCUSSION

In the following, the general characteristics of the measured electron-energy spectra are presented and discussed. Since xenon exhibits a more rich and complex spectrum than those characteristic of the other rare gases, the features specific to this case will be emphasized in the discussion below.

A. Above-threshold ionization in rare-gas electron spectra

Figure 3 illustrates typical electron time-of-flight spectra recorded at a peak laser intensity of $\sim 5 \times 10^{14}$–10^{15} W/cm^2 for helium, neon, argon, and krypton along with a spectrum for xenon corresponding to an intensity of $\sim 5 \times 10^{13}$ W/cm^2. Also shown are the relevant energy-level diagrams[26] with the multiphoton transitions and the electron emission lines indicated. The gas density was adjusted to keep the total electron production below ~ 1000

per pulse.

Several features of the data are apparent. In addition to the prominent lowest-order ionization lines corresponding to the absorption of two photons by xenon, three photons by krypton and argon, and four photons by neon and helium, which leave the corresponding ions in the ground $ns^2np^5\,^2P^o_{3/2}$ or for helium the $1s\,^2S_{1/2}$ states, several above-threshold ionization lines are present. The intensity of the observed ATI lines, however, drops rapidly with increasing order. Only in the case of xenon is a resolved line present indicating that the first ion (Xe^+) is left in its lowest excited state $ns^2np^5\,^2P^o_{1/2}$.

Several relevant experimental parameters are summarized in Table I. The measured ionization-threshold laser intensities are well below the actual peak intensities corresponding to these spectra, a fact which places them well into the saturation regime in which the electron yield grows much slower with increasing laser intensity than that characteristic of the threshold region due to depletion of neutral atoms in the interaction region.[27] This means that most of the single charged ions may be formed before the laser peak intensity is attained in the experimental volume.

The experimental linewidth, if obtained under condi-

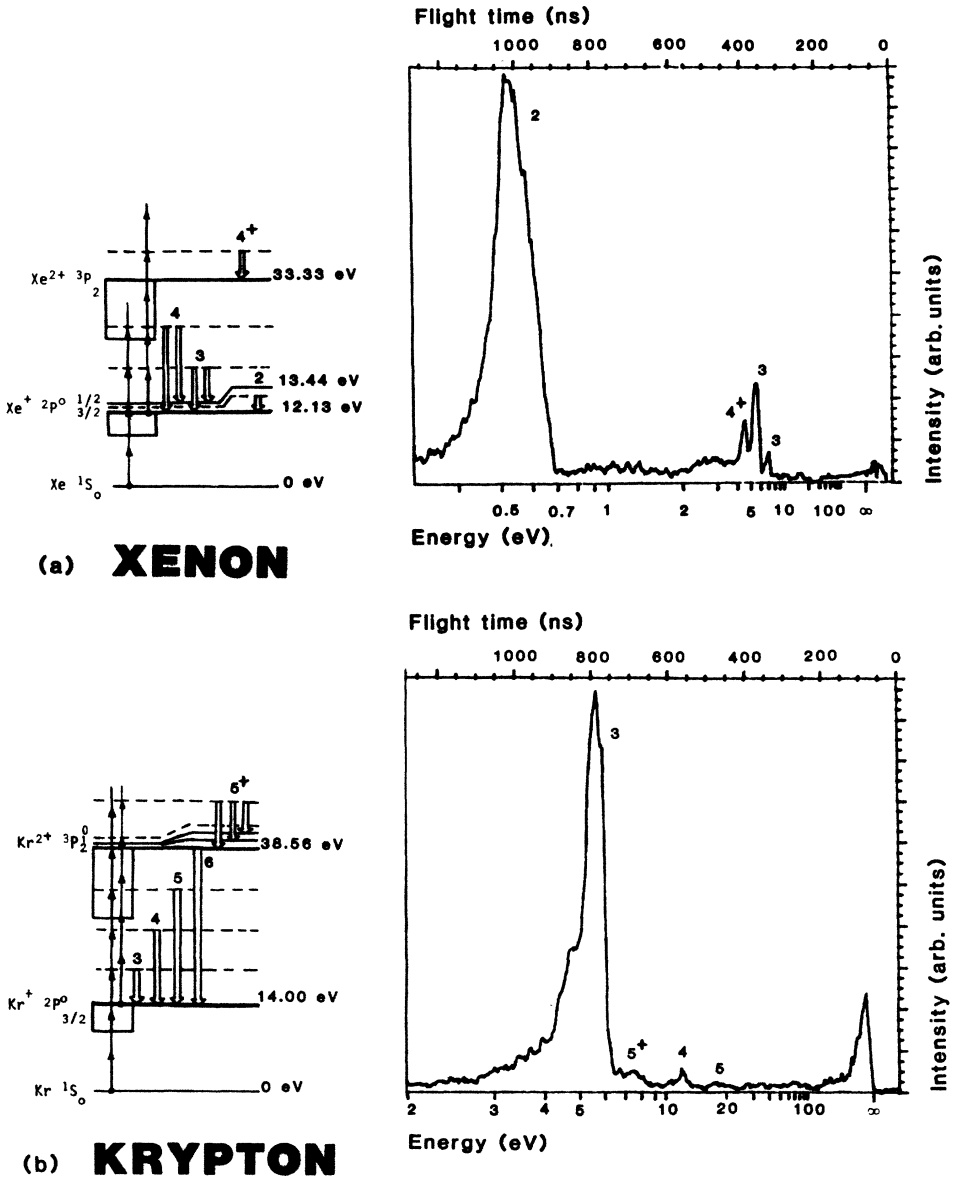

FIG. 3. Typical electron time-of-flight (TOF) spectra for Xe, Kr, Ar, Ne, and He irradiated with a 193-nm laser pulse of ~5 ps duration. The line identification is given in the schematic energy-level diagrams showing relevant energy levels, multiphoton transition (single arrows), and electron emission lines (double arrows). Excited neutral and ionic configurations are indicated by the boxes below the ionization limits. Background lines are labeled as *BG*. The "prompt" line generated by scattered 193-nm radiation impinging directly on the channel plate is followed by a group of photoelectrons produced on the accelerating grid placed in front of the detector. The experimental parameters associated with these spectra are listed in Table I. The inset in the Ar TOF spectrum was taken with a retarding voltage of −2 V. The intensity of the line at ~3.3 eV is underestimated in this recording.

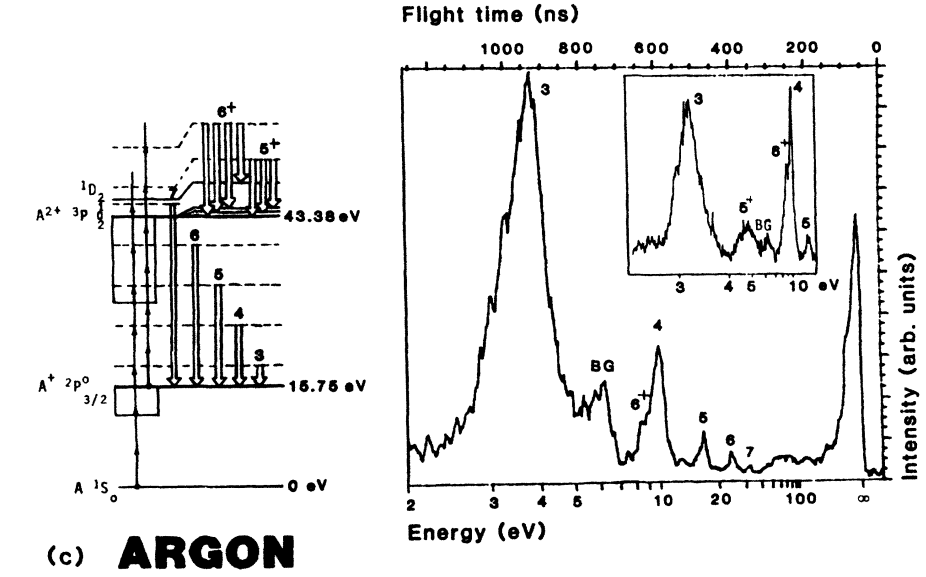

(c) **ARGON**

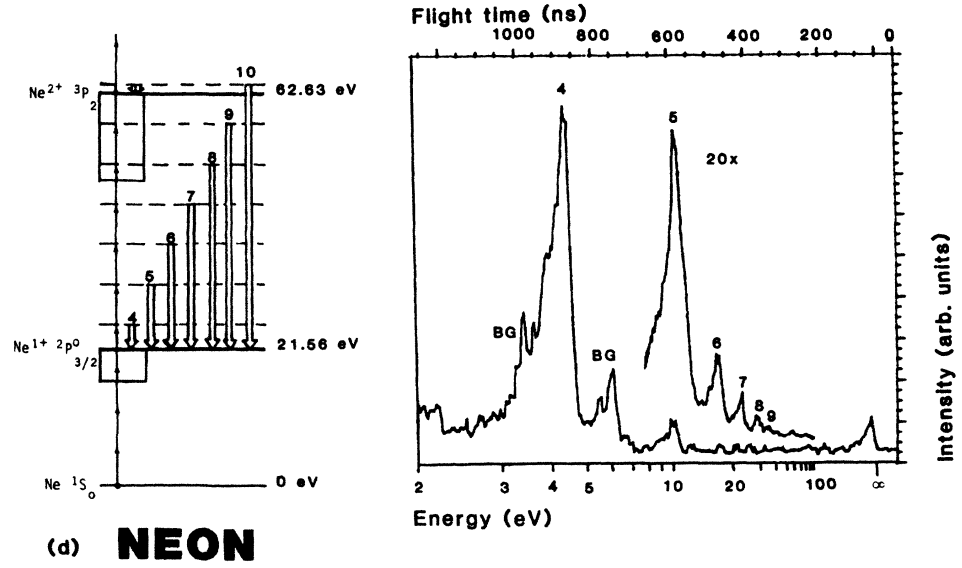

(d) **NEON**

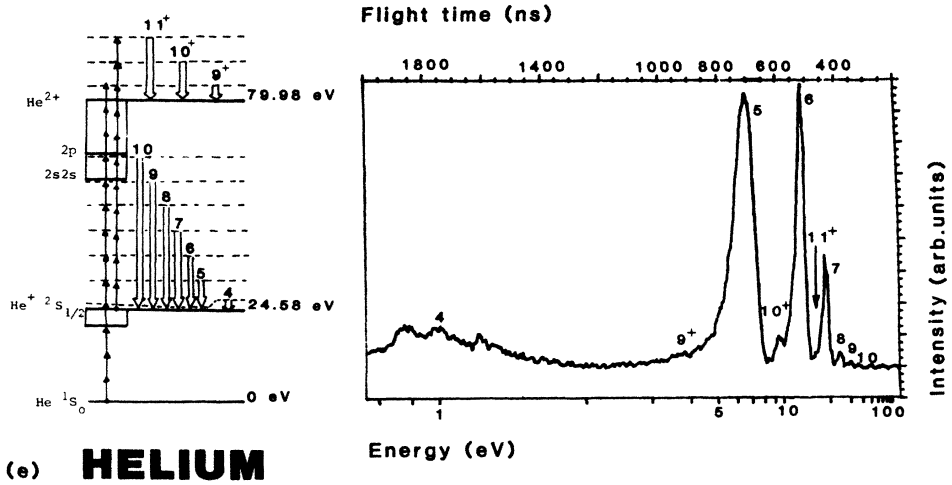

(e) **HELIUM**

FIG. 3. (*Continued*).

TABLE I. Typical experimental parameters for photoelectron ATI ladder lines observed in the ionization of neutral rare-gas atoms. The energy shift is caused by space charge induced by scattered radiation. The calculated threshold laser intensity is defined for a probability of $T=5\times10^{-3}$ (detection limit) and based on the Keldysh model (Refs. 28 and 29).

Element	Laser intensity (W/cm^2)	Gas pressure (Torr)	Threshold laser intensity (W/cm^2) Experimental	Calculated	N photons absorbed	Calculated electron energy (eV)	Experimental electron energy (eV)	Half width (meV)	Relative intensity (%)
Helium	$\sim5\times10^{14}$	5×10^{-6}	$\sim1\times10^{14}$	3.5×10^{14}	4	1.06	1.7(1)	~400	60
					5	7.47	7.9(2)		100
					6	13.88	14.1(2)		29
					7	20.29			8
					8	26.70			2
					9	33.11			0.2
					10	39.52			0.04
Neon	$\sim5\times10^{14}$	1×10^{-5}	$\sim3\times10^{13}$	2.0×10^{14}	4	4.09	4.58(5)	~400	100
					5	10.50	10.95(10)		9
					6	16.91			1.5
					7	23.32			0.5
					8	29.73			0.2
					9	36.14			0.1
					10	42.55			0.05
					11	48.96			0.02
					12	55.37			0.01
Argon	$\sim5\times10^{14}$	2×10^{-7}	$\sim1\times10^{13}$	5.2×10^{13}	3	3.48	4.03(15)	~300	100
					4	9.89	10.43(10)		12
					5	16.30	16.85(8)		2
					6	22.71	22.80(5)		0.8
					7	29.12			0.2
Krypton	$\sim5\times10^{14}$	1×10^{-7}	$\sim1\times10^{9}$	3.1×10^{13}	3	5.24	5.85(10)	~250	100
					4	11.65	12.02(15)		2.5
					5	18.06	18.70(5)		<0.1
					6	24.47			$\ll0.1$
Xenon	$\sim2\times10^{13}$	4×10^{-7}	$\sim1\times10^{10}$	1.5×10^{13}	2	0.69	0.72(5)	~230	100
					3	5.79	5.92(10)		4
					3	7.10	7.24(10)		0.8
					4	12.20			<0.04
					4	13.51			<0.04

tions of high resolution for which space-charge broadening is minimized, is found to be between 250 and 500 meV for all lines at the highest laser intensities used in these studies, and decreases to about 50–200 meV close to the threshold. Factors that could contribute to excessive broadening are shot-to-shot fluctuations of the line positions and laser intensity and the influence of dynamic Stark shifts of atomic levels caused by varying field intensities over the interaction volume.

Table I also contains a comparison of the measured threshold intensities with values calculated according to the Keldysh-Raizer formula in the multiphoton ionization limit.[28,29] This formulation gives

$$W=B\omega N_{\min}^{3/2}(e^2\mathbf{E}_0^2/8m\omega^2T_0)^{N_{\min}} \tag{3}$$

in which W is the transition rate, B is a factor of order unity, $N_{\min}$ is the minimum number of photons with quantum energy ($\hbar\omega$) necessary to overcome the generalized field-dependent ionization threshold $T(\mathbf{E})$ discussed in following Sec. III B 1, T_0 is the usual ionization threshold, and $\mathbf{E}_0$ is the laser electric field amplitude. The transition probability P then becomes

$$P=W\tau_p \tag{4}$$

in which τ_p denotes the laser pulse length. Reasonable agreement is found with this formula for He, Ne, and Ar. In contrast, the experimental values are considerably lower than the corresponding Keldysh values for both Kr and Xe. The threshold intensity is defined in these calculations as that necessary to produce a one-electron signal per laser pulse at the detector. Clearly, the influence of atomic resonances is responsible for the lower thresholds observed in Kr. In this case, a set of three known[30] two-photon near resonances exists involving transitions from the $4s^24p^6$ ground state to those with the excited configuration $4s^24p^56p$. The energy parameters describing the detuning from exact resonance are small with values of $\delta\varepsilon\approx-6$, -36, and 44 meV, respectively. One of these transitions, occurring in the overall process

$$4s^24p^6\,{}^1S_0+2\gamma(6.41\text{ eV})\rightarrow4s^24p^5({}^2P^{\circ}_{3/2})6p+1\gamma \rightarrow4s^24p^5\,{}^2P^{\circ}_{3/2}+e^-(5.25\text{ eV}), \tag{5}$$

strongly favors the excitation channel leading to the $J=\frac{3}{2}$ core level, the state corresponding to the ground ionic term. In comparison, the more off-resonant channel

$$4s^2 4p^6\,{}^1S_0 + 2\gamma(6.41\text{ eV}) \rightarrow 4s^2 4p^5({}^2P^{\circ}_{1/2})6p + 1\gamma \rightarrow 4s^2 4p^5\,{}^2P^{\circ}_{1/2} + e^-(4.56\text{ eV}) , \tag{6}$$

with detuning $\delta\varepsilon \sim 630$ meV, leads to formation of the ion in the first excited state. Thus, the near resonance in process (5) explains the absence or the weakness of the 4.56-eV electron line corresponding to reaction (6) in the Kr spectrum. A similar situation holds for Ar, in which a two-photon near resonance, with upper-level configuration $3s^2 3p^5 4p$ and detuning parameter $\delta\varepsilon \sim 85$ meV, may enhance ion ground-state formation in the process

$$3s^2 3p^6\,{}^1S_0 + 2\gamma(6.41\text{ eV}) \rightarrow 3s^2 3p^5({}^2P^{\circ}_{3/2})4p + 1\gamma \rightarrow 3s^2 3p^5\,{}^2P^{\circ}_{3/2} + e^-(3.48\text{ eV}) . \tag{7}$$

It should be noted, however, that the energy of detuning can change significantly at high laser fields due to the dynamic Stark shift, a fact that can significantly alter resonance effects[31,32] of this kind.

The situation is complicated in xenon by the fact that the two-photon energy (12.82 eV) falls in the energy region containing the autoionizing Rydberg series which converges to the excited $5s^2 5p^5\,{}^2P^{\circ}_{1/2}$ ion state. Because of the rather close spacing of Rydberg levels, near resonances occur in this region. For example, the observed[33] even-parity state.

$5s^2 5p^5({}^2P_{1/2})5f\,{}^1[\frac{5}{2}]_2$, which falls at 12.886 eV, has a weak-field detuning parameter of only $\delta\varepsilon = +64$ meV. This level, as well as other even parity states, could have an appreciable influence on the overall transition rate.

In xenon with 193-nm radiation, sufficient energy is available to populate both the ionic $^2P^{\circ}_{3/2}$ ground state and the corresponding $^2P^{\circ}_{1/2}$ excited state with three- and four-photon absorption. Interestingly, the observed branching ratio ($R_N \equiv R_{^2P^{\circ}_{1/2}}/R_{^2P^{\circ}_{3/2}}$) for the corresponding electron line intensities I_e gives

$$R_3 = I_e(5.79\text{ eV})/I_e(7.10\text{ eV}) \sim 5$$

and

$$R_4 = I_e(12.20\text{ eV})/I_e(13.51\text{ eV}) \sim 4 .$$

This indicates a strong enhancement of the channel forming the excited $^2P^{\circ}_{1/2}$ state, a finding that strongly contrasts with the statistical value of 0.5 and the measured ratio of 0.62 for single-photon ionization at a comparable total energy.[34] Branching ratios in other multiphoton experiments have been reported to be $R_5 \sim 1$ for five-photon absorption[35] at $\hbar\omega = 2.81$ eV and $R_N = 1.35$, 0.43, and 0.3 for six-, seven-, and eight-photon absorption of $\hbar\omega = 2.34$ eV, respectively.[12] Apparently, several factors, including the laser intensity, the presence of near resonances, and the order of the process influence the value of this ratio.

Since the experimental results provide information on the relative intensities of the electron lines originating from ATI processes of different order N, a comparison to other studies performed under different conditions can be made. As shown in Table I, a more rapid decrease is observed in the ultraviolet region at 193 nm as compared to the corresponding results obtained at visible and infrared wavelengths.[12,13] On the basis of the linear density dependence observed for the intensities of the electron lines, inverse bremsstrahlung heating in the plasma as the mechanism producing the higher-order electron lines was found to be insignificant at least up to pressures of $\sim 10^{-5}$ Torr, the highest values used in these experiments. The signature of the bremsstrahlung mechanism would have been a quadratic dependence of the electron intensity on gas density.

Examination of the intensity distributions on the ATI lines also indicates that the highly excited configurations of the neutral atoms occurring above the first ionization threshold, as well as levels of excited ionic configurations, do not appreciably affect the rates of ionization for the observed channels. The boxed regions shown on the energy-level diagrams in Fig. 3 indicate the range of energies in which levels of excited ionic configurations occur. Although it is seen in all five cases that these regions overlap the energies associated with certain observed ATI features (e.g., $N=8,9$ in Ne and $N=5,6$ in Ar), the intensities observed for these lines do not exhibit anomalous variations in comparison with other electron lines falling outside these specific energy regions.

Theoretical values for the relative probabilities of ATI lines have been calculated by Chu and Cooper[36] for hydrogen. Other analyses describing the dynamics of the process have been given by Crance and Aymar[37] and by Gontier and Trahin[38] who assume a well-defined spatial and temporal intensity distribution for characterization of the laser beam. Although a quantitative comparison of our data with these calculated hydrogenic probabilities is not strictly valid because of experimental uncertainties and the electronic complexity of the rare-gas atoms as compared to hydrogen, the experimental results qualitatively reflect the behavior predicted by the earlier work of Chu and Cooper[36] and Gontier and Trahin.[38]

Briefly, at ultraviolet wavelengths, relatively low-order processes (e.g., $N=2$ and 3) can energetically lead to ionization of the neutral system for most materials. Because of this, the intensity level needed to produce an ionization rate comparable to the inverse of the pulse width, a condition that leads to saturation, is relatively low. Indeed, resonances in the amplitude, such as those noted above for argon, krypton, and xenon with 193-nm radiation, can further reduce this requisite intensity for rapid ionization. Consequently, during the rise time of the laser pulse, a substantial fraction of the atoms can become ionized into the first ionization channel before the intensity becomes sufficiently great to produce a comparable transition rate for higher-order processes. For longer wavelengths, which require a higher-order process to accomplish ionization, it is anticipated that the saturation intensity for ionization and the intensity required for comparable ATI transition rates will have values that are closer together.

In addition, if the ATI process is pictured physically as an inverse-bremsstrahlung mechanism involving the intimately associated electron-ion pair, the absorption rate at shorter wavelengths is expected to be suppressed in comparison to longer ones[39] because of the wavelength dependence of the absorption coefficient which, in standard form, is proportional to the square of the wavelength. Therefore, it is expected, at ultraviolet wavelengths, that the enhancement of the higher-order processes of absorption requires a sharp rise time of the ultraviolet pulse. This condition, which is examined further below in Sec. III B 5, enables the intensity experienced by the atom to reach values of a sufficient magnitude in a sufficiently short time so that higher-order channels can compete effectively with those of lower order. In the present experiments, the requirements of this condition do not appear to be well fulfilled. Highly-charged ions, however, because of the significantly increased energy of ionization, may tend to exhibit more-pronounced ATI absorption, since the order N of the lowest ionization channel is greater, a condition that will generally lead to an increased saturation intensity. The same consideration applies in the comparison of the strengths of the higher-order features of the ATI spectra of the rare gases which are observed to increase in the expected fashion (Table I and Fig. 3) from Xe to He.

Multiply excited atomic states may play an important role in the many-quantum absorption process, particularly if sufficient intensity can be rapidly applied to the atom, and if appropriate resonances with multiply excited levels are present in the amplitude. Indeed, a picture based on a collective atomic response involving several electrons occupying excited orbitals has been considered in certain models.[40,41,42] These analyses display features which are, in principle, compatible with the extant experimental data.[3,4]

Specific detailed information is available for helium, argon, krypton, and xenon for low-lying multiply excited levels in the region below 50 eV. In krypton, the multiply excited manifold begins at $\sim$23.3 eV above the neutral ground state[44,45,46] and is, therefore, reached by a four-quantum process at 193 nm (25.65 eV). We note that the excited states in this region have been strongly implicated in the recent study[47,48] of radiative mechanisms exhibited by krypton under excitation at 193 nm. For argon, $3s$ inner-shell excitation begins at 26.61 eV and doubly excited levels exist[43] above 29.0 eV. For xenon, autoionizing levels corresponding to single $5s$-shell excitation and double $5p$-shell excitation have been observed[44] above $\sim$20.95 eV. Interestingly, although levels in krypton with single $4s$-shell excitations and double $4p$-shell excitations may play a role in the radiative response[47,48] for 193 nm intensities in the range of $\sim 10^{12}$–10^{14} W/cm^2, no clear evidence for the influence of these states on the ATI ladder lines was observed in the electron spectra at an intensity of $\sim 5\times 10^{14}$ W/cm^2, as shown in Table I. Similarly, as noted above, for helium, neon, argon, and xenon the observed ATI pattern did not give evidence of substantial influence arising from the known multiply excited levels. If the intensity of the ATI electron lines is interpreted as a measure of the photon absorption rate for higher-order processes, only a fraction on the order of 1% or less of the higher charged ion states produced could be attributed to this type of direct excitation mechanism under the given experimental conditions.

B. Additional lines in the rare-gas electron spectra

A question of principal significance concerns the identification of the dominant mechanism responsible for the production of highly charged ions under collision-free irradiation.[49] The sequential stripping of single electrons with increasing laser intensity,[50] a stepwise process which leaves the ions in their ground or low excited states, should generate an electron-energy spectrum consisting of a group of sharp lines which accompanies the normal ATI ladder series associated with the neutral ground state. In an alternative process involving the direct multiple autoionization or photoionization of multiply excited states, the liberated electrons can mutually redistribute the excess energy available and generate a continuous component of relatively low-energy electrons to the measured spectrum. In addition, atomic intershell energy transfer may occur in which energy associated with the excitation of outer-shell electrons can be communicated to inner shells by an interaction that has been pictured as a form of dynamic configuration interaction.[19,20] The inner-shell excited states produced could subsequently decay radiatively or by the emission of Auger electrons with characteristic energies.

Experimentally, all of these different excitation and decay channels can occur simultaneously in the interaction region, a situation which may seriously complicate the interpretation on the observed electron-energy spectra. Some simplification, however, arises from the use of ultraviolet quanta because the characteristic spacing that occurs between ATI lines is relatively large, a factor that more readily permits resolution of fine details in the spectrum.

Evidence for the presence of the sequential process is shown in Fig. 3(a) for xenon. In this case, at an intensity of $\sim 2\times 10^{13}$ W/cm^2, a weak line at 4.44 eV is observed which indicates the formation of the Xe^{2+} $(5s^25p^4)^3P_2$ ground state which arises from a four-photon absorption from the Xe^+ $(5s^25p^5)^2P^\circ_{3/2}$ ionic ground level. Upon an increase in the 193-nm laser intensity, the energy distribution of the electrons observed in the xenon spectrum changes dramatically, as shown in Fig. 4, a low-resolution time-of-flight recording spanning the energy range between $\sim$0.3 and 100 eV. It is seen that the lowest-order ionization line weakens and splits nearly symmetrically into two features whose separation grows with increasing intensity. At the greater intensity, the line group around 5 eV, comprised of the two three-photon ATI ladder lines and the four-photon line indicating the sequential Xe^{2+} ground-state formation, begins to dominate the spectrum. In addition, a broad quasicontinuous feature at $\sim$3 eV and new line groups between $\sim$8 eV and 30 eV are apparent. In Fig. 5, the Xe spectrum is displayed with high resolution at an intensity of $\sim 10^{15}$ W/cm^2 and converted to a linear energy scale. More than twenty sharp lines are visible in this spectrum. In order to interpret this com-

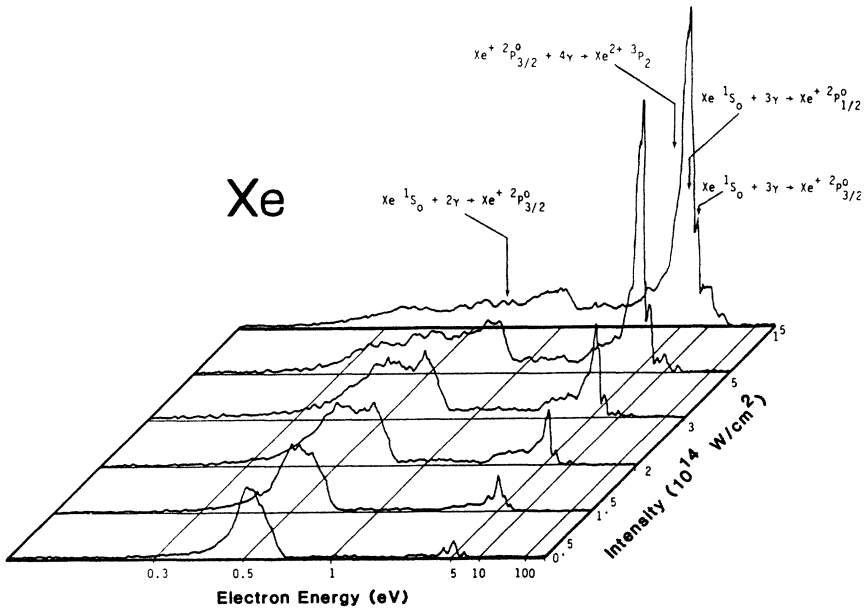

FIG. 4. Laser intensity dependence of the Xe TOF electron spectrum recorded at low-energy resolution (no retardation). The electron-energy range spanned is between ~0.3 and 100 eV.

plex spectrum, several physical effects have to be considered.

1. Shift of ionization thresholds. The weakening of low-energy photoelectron lines with increasing laser intensity has been reported by Kruit *et al.*[13] in experiments at 1.06 μm. Subsequently, several theoretical papers have appeared giving descriptions and explanations of this effect.[36,51–55] In the discussion below, we adopt the analysis developed by Szöke.[56]

The energy conservation governing the motion of an electron undergoing photoionization by a multiphoton process in an intense, linearly polarized electromagnetic

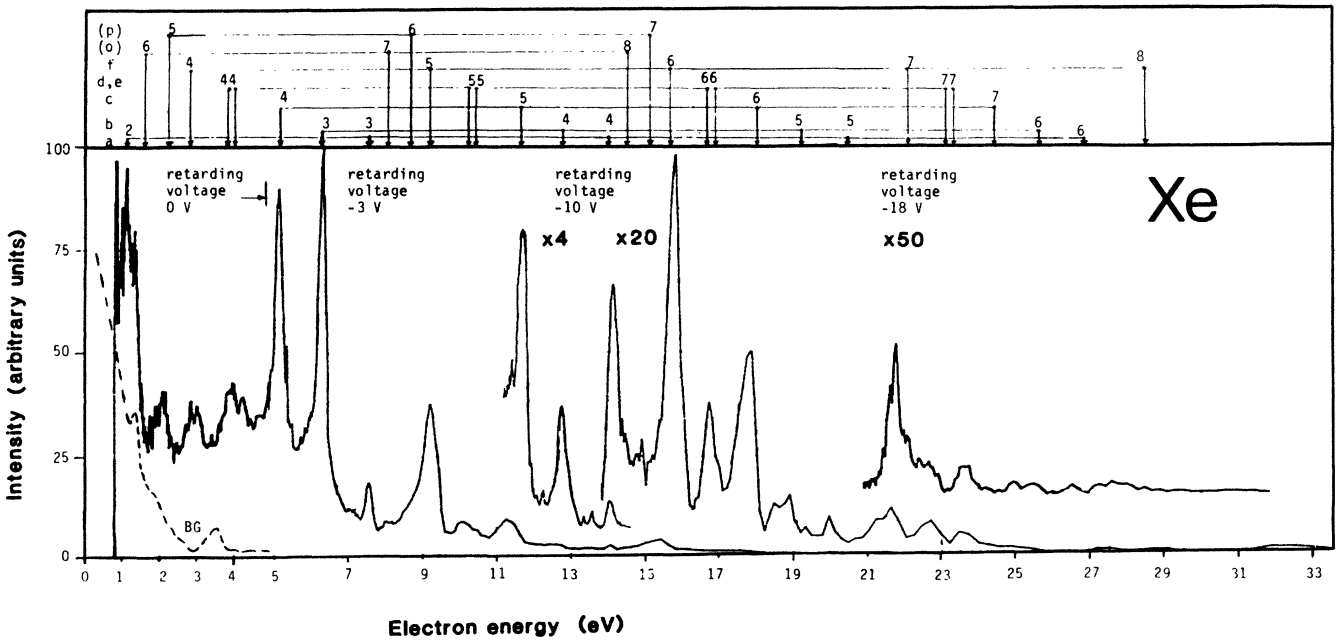

FIG. 5. High-resolution Xe electron-energy spectrum recorded at a 193-nm laser intensity of ~10^{15} W/cm^2 and a gas pressure of ~4×10^{-7} Torr. The energy scale has been calibrated at low laser energy, where the lines are unshifted (see text). The vertical scale multiplication factors are approximate and refer to the integral number of electrons observed in the corresponding energy interval. The identification of the lines with their respective above-threshold ladder series is shown on top of the spectrum. The letter labeling refers to the specific sequential processes listed for Xe in Table III to which the main component of the observed ladder is attributed. The associated number indicates the number of the photons absorbed.

field is expressed by the relation

$$\varepsilon_D(N) \equiv \varepsilon_{A,q}(\mathbf{E}) + N\hbar\omega = \varepsilon_{A,q+1}(\mathbf{E}) + \frac{1}{4}\frac{\mathbf{E}_0^2 e^2}{m\omega^2} + \frac{\mathbf{P}^2}{2m} . \tag{8}$$

In expression (8) $\varepsilon_D(N)$ is the energy of the "dressed" atom (ion) state and $\varepsilon_{A,q}(\mathbf{E})$ and $\varepsilon_{A,q+1}(\mathbf{E})$ are the energies, respectively, of the initial state of the q-charged ion and the final state of the $(q+1)$-charged ion in the electromagnetic field $\mathbf{E}$. Both states are shifted in energy by the dynamic Stark effect by amounts given by

$$\Delta\varepsilon_{A,q}(\mathbf{E}) \equiv \varepsilon_{A,q}(\mathbf{E}) - \varepsilon_{A,q}(0) \tag{9}$$

and

$$\Delta\varepsilon_{A,q+1}(\mathbf{E}) \equiv \varepsilon_{A,q+1}(\mathbf{E}) - \varepsilon_{A,q+1}(0) \tag{10}$$

from their zero-field energy. This effect is usually small (<100 meV) for the more tightly bound initial states (ground levels) of the rare gases. The last two terms represent the total motional energy of the electron, which consists of the piece described by the pondermotive potential, which arises from the oscillatory motion of the electron in the alternating field, and the term denoting the translational energy with momentum $\mathbf{P}$. The oscillating motion of the ion[55] is neglected in this expression, since its large mass causes that contribution to be small. Once the electron is outside the influence of the ionic Coulomb field, it cannot emit or absorb real photons. It has been previously shown[56] that the influence of Compton scattering is negligible under the conditions relevant to these experiments. Therefore, the total energy of the electronic motion is conserved and the component represented by the rapidly oscillating quiver motion is converted into translational kinetic energy by the ponderomotive force[57] as the particle moves to the zero-field region ($\mathbf{E}\rightarrow 0$) on its way to the detector.

The essential point here is that if the electron is excited to a total energy in the continuum *less* than that associated with the ponderomotive potential, namely, the quiver energy under those field conditions, it cannot escape from the Coulomb potential and is trapped. This is equivalent to stating that the ionization or continuum threshold, which can be defined as the series limit characterizing the liberation of a Rydberg electron from a dressed state, is upshifted by an amount equal to the quiver energy. Therefore, the expression

$$T(\mathbf{E}) = T_0 + \frac{1}{4}\frac{\mathbf{E}_0^2 e^2}{m\omega^2} + \Delta\varepsilon_{A,q+1}(\mathbf{E}) - \Delta\varepsilon_{A,q}(\mathbf{E}) , \tag{11}$$

in which $T_0 = \varepsilon_{A,q+1}(0) - \varepsilon_{A,q}(0)$ is the usual low-field ionization threshold, can be considered as a generalized ionization threshold. The principal consequence of this condition is the closing of low-energy ionization channels above certain characteristic laser intensities. This effect has been discussed earlier by Keldysh[28] and Raizer.[29] Furthermore, since the total energy of the electron after the multiphoton absorption event is conserved, its deficit in translational kinetic energy in the high-field region is regained upon expulsion from that zone, leaving its kinetic energy altered relative to a low-field event only by the small difference arising from the dynamic Stark shifts of the initial and final atomic or ionic states. This situation holds for the condition that the escape velocity of the electron out of the focal region is sufficiently fast with respect to the rate of variation of the laser intensity.[56]

Consequently, as the peak intensity of irradiation is increased, the lower-energy ionization channels close and the spectrum of emitted electrons shifts towards the higher-order lines while the line positions remain nearly unaffected. It should be noted, however, that a perceptible shift of the electron spectrum could already occur before the lower-energy channels close.[36,38,52,54] Further, because of the ω^{-2} dependence of the ponderomotive potential, the radiative influence on the shift of the ionization threshold is considerably stronger in the infrared region than in the ultraviolet.

Interestingly, energetic electrons have been observed in experiments conducted at 1.06 μm at a peak intensity of $\sim 10^{16}$ W/cm^2. In these relatively-low-resolution studies,[8,17] performed by Baldwin, Boreham, and Luther-Davis, electrons with energies up to several hundred eV were detected and the origin of their acceleration was attributed to the ponderomotive force. However, the unshifted line positions observed by Kruit and co-workers[13] seem to be at variance with this result. In this connection it is noted that, due to the upshift of the ionization threshold by the ponderomotive potential, the lowest ionization channel open for 1.06-μm radiation at this intensity corresponds to a transition involving several hundred photons. Of course, low-energy electrons are simultaneously observed as a result of ionization early in the rise of the pulse or from generation in peripheral regions of the interaction volume that are exposed to a lower intensity. Similar findings have been recently reported by Lompré and co-workers[16] who observed, in low-energy resolution experiments, electrons with energies up to 50 eV. In this case,[16] it was assumed that the virtual excitation of multiply excited states enhanced the probability for ATI processes. However, this analysis did not take into account the radiative shift of the ionization threshold.

The relative weakening of the two-photon (0.7-eV) ionization line and the related strengthening of the three-quantum ionization lines observed in the xenon electron spectrum can probably be attributed to the closing of the lower (0.7-eV) channel throughout a considerable fraction of the interaction volume. The intensity of 193-nm radiation necessary to shift the ionization threshold an energy equivalent to 0.7 eV is $\sim 2\times 10^{14}$ W/cm^2, a value in good agreement with our experiment. A substantial relative suppression of the lowest four-photon absorption ionization line has been found for helium, as is evident from Table I and Fig. 3(e). According to Eq. (11), this ionization channel, 1.06 eV above the unshifted ionization threshold, should close at a laser intensity of 3×10^{14} W/cm^2, a value close to the measured threshold intensity of $\sim 1\times 10^{14}$ W/cm^2, supporting the interpretation as a ponderomotive force effect.

2. Dynamic Stark splitting of the Xe two-photon ionization line. The splitting of the two-photon ionization line at ~ 0.7 eV in xenon illustrated in Fig. 6 that develops

with increasing 193-nm intensity occurs in the intensity range between $\sim 10^{10}$ and 10^{12} W/cm^2. Since these intensities are rather lower, the splitting is readily observed with the relatively-low-power ASE pulse ~ 10 ns duration without the presence of the considerably more intense picosecond radiation. The experimental signature of the splitting appears to rule out a spurious instrumental origin for this effect. The splitting is seen to be independent of both pressure and the position of the interaction region along the magnetic field axis. The influence of space charge generated by scattered 193-nm radiation from surfaces has been examined by independently illuminating the surfaces near the interaction zone with a separate beam. As a result of the charge density produced in this way, the line is shifted to higher electron energy with a perceptibly altered shape, but importantly, with the splitting preserved.

As noted above, the two-photon absorption in xenon is distinguished by the fact that the equivalent two-photon energy is located in the autoionizing Rydberg series converging to the $5s^2 5p^5\,{}^2P^o_{1/2}$ series limit, a property leading to the presence of near-resonances.[58] It is well known that if a sufficiently strong coupling is established between two states by an intense resonant field, a splitting can develop which arises from the dynamic Stark effect of the dressed atomic states.[59] In case the upper state is an autoionizing level, the influence of the Autler-Townes effect on the electron-energy spectrum has been studied extensively by Rzażewski and Eberly[60] for a transition involving a single photon. Moreover, this dynamic Stark splitting, in the context of multiphoton transitions and electron-energy spectra, has been discussed by Lambropoulos and Zoller[1(a)] and Bialynicka-Birula.[54] Both the near-resonant discrete state and the continuum are coupled to each other by the Coulomb interaction as described by Fano.[61] The energy distribution of the photoelectrons released from the autoionizing state acts as a probe to detect the splitting. The actual shape of the resulting photoelectron line depends sensitively on the parameters governing the behavior of the system. The relevant parameters are the radiative coupling strength linking the two resonant levels, the autoionization linewidth, the laser bandwidth, the pulse length, the dephasing rate, the intensity-dependent detuning of the laser from the discrete resonances, and the Fano asymmetry parameter. We tentatively interpret the observed splitting of the 0.7-eV line in xenon as arising from the dynamic Stark effect. By fitting the measured line profile to the parameters mentioned above, the observed electron line shape, including the intensity dependence, could be reproduced for parameters representing reasonable physical values. A more detailed analysis will be published elsewhere.

3. Evidence concerning high charge-state production. Table II lists the relative ion charge-state abundances for Xe, Kr, and Ar which have been obtained previously in an ion time-of-flight experiment,[3,4] under conditions which are similar to those of the present electron-energy measurements. Based on these charge-state distributions, the calculated relative electron yield expected for (a) a purely sequential and (b) a purely direct process, respectively, is shown in the same table. According to this comparison,

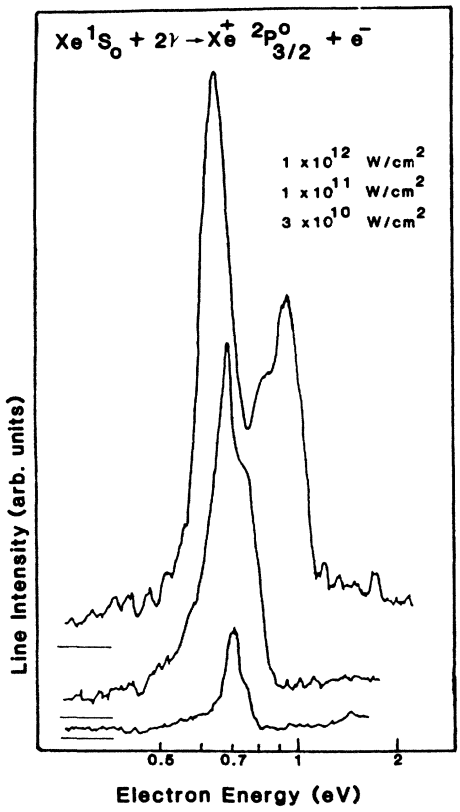

FIG. 6. Splitting of the two-photon 0.7-eV-electron emission line observed in xenon as a function of increasing 193-nm intensity at a gas pressure of $\sim 10^{-6}$ Torr. Only the 10-ns ASE component of the 193-nm laser pulse was used for excitation.

in the direct process, approximately 70% for xenon, 30% for krypton, and 15% for argon of all electrons that are produced arise from the formation of higher charged ions. It is expected that these electrons would contribute a relatively low-energy continuum to the electron spectra. No unambiguous evidence for the existence of such a contribution to the continuum has been found, but its presence could be obscured by the surface background electrons produced by scattered radiation and the low-energy wings of the prominent ATI ladder lines shown in Fig. 3. The gas density has been kept low in order to avoid detector saturation caused by the higher-energy lines. The possibility that these electrons are trapped in the space charge of the residual ion cloud was tested and ruled out by the application of a static electric field across the interaction region.

If the model of sequential electron production is adopted, several channels for ionization have to be simultaneously considered because of the number of possible excited states that could be produced in conjunction with the distribution of the observed ionic species. Table III lists some of the processes which are believed to be significant. They are, in the case of xenon, related to the observed lines illustrated in Fig. 5. As shown in the figure, the lines which are manifest in the measured xenon electron energy spectrum for intensities above $\sim 2\times 10^{14}$ W/cm^2

TABLE II. Relative ion charge state abundance for Xe, Kr, and Ar obtained in an ion time-of-flight experiment (Refs. 3 and 4) under conditions comparable to the present electron data. Based on this distribution, the expected relative electron yield from the production of each charge state in purely sequential or direct processes, respectively, has been calculated.

Element	Relative abundance (%)	Ion charge state 1+	2+	3+	4+	5+	6+
Xenon	Ions	49	31	17	2.6	1.1	0.27
	Electrons sequential	56	29	12	2.2	0.8	0.15
	Electrons direct	27	35	28	6	3	1
Krypton	Ions	82	14	3.3	0.3		
	Electrons sequential	82.3	14.5	2.7	0.25		
	Electrons direct	68	23	8	1		
Argon	Ions	91	9				
	Electrons sequential	92	8				
	Electrons direct	84	16				

closely match a pattern of overlapping ATI ladder series with each series associated with the population of a respective ionic state. The branching ratios for the different excited states of the residual ions are not known and, as discussed in Sec. III A preceding, may depend strongly on intensity-dependent resonances. We note the accidental coincidence of several line energies, a fact which makes it difficult to isolate certain individual ladder contributions, especially those for processes leading to Xe^{3+} and higher charge states. The lowest energy lines are seen to be grouped in the range between ~ 2 and 6 eV. More energetic groups are apparent with corresponding spacings of lines given approximately by the photon energy of 6.41 eV. Estimates of the relative intensities for the most prominent lines are listed in Table IV. Except for the first group of lines in the 2—4-eV range shown in Fig. 5, the relative line intensity within each of the higher energy groups is repeated, although the absolute intensity of these features drops rapidly with increasing energy. At a density of $\sim 2\times 10^{-5}$ Torr, weak line groups up to an energy of ~ 60 eV could be observed in this experiment.

These data indicate that in the sequential production of the higher charge states of the xenon ions, ATI occurs with a greater probability than in the multiphoton ionization of the neutral xenon atom. This observation may be attributable to the higher saturation intensity expected to be characteristic of the ionized species resulting from the larger energy of ionization and the correspondingly greater order N of the threshold process. The comparison of the relatively weak group of lines in the 2—4-eV region of Fig. 5 with those lines of the next higher order indicates that the lowest-order channels close, at least for the maximum intensity region of the interaction volume. The closing of these channels corresponds to a range of intensities spanning from $\sim 5.6\times 10^{14}$ W/cm^2 (~ 2 eV) to $\sim 1.4\times 10^{15}$ W/cm^2 (~ 5 eV). This closing of the lowest-order channels of ionization could explain the fact that the lowest energy feature (f5) in the next-higher-order group is the most intense. A close examination of the line energies reveals that the individual ATI ladder series are shifted in energy relative to each other by an amount on the order of ~ 50 meV. Although these apparent shifts have to be interpreted with caution, since they may be subject to the influence of space charge induced by scattered radiation, they may represent the relative dynamic Stark shifts of the initial and final ionic states according to Eq. (11).

The total integrated intensity of the neutral ionization lines is approximately equal to that of the ionization lines arising from the ions. As presented in Table II, the sequential process can account for the total ion production observed in xenon to within the experimental uncertainty. The question of the existence of an additional continuum contribution underlying the densely packed features between 0.5 and 6 eV, although possible, cannot be answered with the energy resolution available in this experiment. L'Huillier and co-workers[62] concluded from their experimental ion data that direct excitation of the neutral atom is the dominant process at intensities below the saturation level. Above that intensity, due to the depletion of neutral atoms in the interaction volume, the sequential ionization of ions becomes increasingly important.[50] This view is not in conflict with the results of the present work, since the spectra were taken well in the saturation regime. The direct excitation process could become significant at ultraviolet wavelengths for the production of charge states higher than the triply charged ion, because the situation for these species, as noted in Sec. III A preceding, is similar to that governing the interaction of atoms with infrared fields.

More information concerning the competition between the sequential and direct processes should be obtainable from a study of the electron spectra of the other rare gases. The behavior of xenon contrasts with that exhibit-

TABLE III. Important multiphoton channels of ionization in the production of xenon, krypton, and argon charge states by the sequential mechanism. The electron energy (in eV) is the calculated excess energy above the residual ion state energy and refers to the number of photons absorbed in the ATI process. The last column shows the experimental energy shift for xenon (in meV) of different ATI ladders normalized to the lowest-order ladder process (a) and obtained after identification with observed lines in the xenon spectrum shown in Fig. 5.

Code	Process					Electron energy (eV)		Energy shift (meV)
					Xenon			
a	Xe	$5s^2 5p^6\,{}^1S_0$	$+2\gamma,3\gamma,4\gamma,5\gamma$	$\rightarrow Xe^{1+}$	$5s^2 5p^5\,{}^2P^\circ_{3/2}+e^-$	0.69, 7.10,13.51,	19.92	0
b			$3\gamma,4\gamma,5\gamma$		${}^2P^\circ_{1/2}+e^-$	5.79,12.20,18.61		40
c	Xe^{1+}	$5s^2 5p^5\,{}^2P^\circ_{3/2}$	$+4\gamma,5\gamma,6\gamma,7\gamma$	$\rightarrow Xe^{2+}$	$5s^2 5p^4\,{}^3P_2+e^-$	4.44,10.85,17.26,	23.67	263
d			$4\gamma,5\gamma,6\gamma,7\gamma$		${}^3P_1+e^-$	3.23, 9.64,16.02,	22.46	56
e			$4\gamma,5\gamma,6\gamma,7\gamma$		${}^3P_0+e^-$	3.43, 9.84,16.25,	22.66	71
f			$4\gamma,5\gamma,6\gamma,7\gamma$		${}^1D_2+e^-$	2.32, 8.73,15.14,	21.55	0
g	Xe^{1+}	$5s^2 5p^5\,{}^2P^\circ_{1/2}$	$+4\gamma,5\gamma,6\gamma,7\gamma$	$\rightarrow Xe^{2+}$	$5s^2 5p^4\,{}^3P_2+e^-$	5.75,12.16,18.57,	24.98	
h			$4\gamma,5\gamma,6\gamma,7\gamma$		${}^3P_1+e^-$	4.54,10.95,17.36,	23.77	
i			$4\gamma,5\gamma,6\gamma,7\gamma$		${}^3P_0+e^-$	4.74,11.15,17.56,	23.97	
j			$4\gamma,5\gamma,6\gamma,7\gamma$		${}^1D_2+e^-$	3.63,10.04,16.45,	22.86	
k	Xe^{2+}	$5s^2 5p^4\,{}^3P_2$	$+6\gamma,7\gamma,8\gamma$	$\rightarrow Xe^{3+}$	$5s^2 5p^3\,{}^4S^\circ_{3/2}+e^-$	6.27,12.78,19.19		
l			$6\gamma,7\gamma,8\gamma$		${}^2D^\circ_{3/2}+e^-$	4.73,11.14,17.55		
m			$6\gamma,7\gamma,8\gamma$		${}^2D^\circ_{5/2}+e^-$	4.20,10.61,17.02		
n			$6\gamma,7\gamma,8\gamma$		${}^2P^\circ_{1/2}+e^-$	2.89, 9.30,15.71		
o			$6\gamma,7\gamma,8\gamma$		${}^2P^\circ_{3/2}+e^-$	1.18, 7.59,14.00		(496)
p	Xe^{2+}	$5s^2 5p^4\,{}^1D_2$	$+5\gamma,6\gamma,7\gamma$	$\rightarrow Xe^{3+}$	$5s^2 5p^3\,{}^4S^\circ_{3/2}+e^-$	2.05, 8.46,14.87		(−374)
					Krypton			
a	Kr	$4s^2 4p^6\,{}^1S_0$	$+3\gamma,4\gamma,5\gamma,6\gamma$	$\rightarrow Kr^{1+}$	$4s^2 4p^5\,{}^2P^\circ_{3/2}+e^-$	5.24,11.65,18.06	24.47	
b	Kr^{1+}	$4s^2 4p^5\,{}^2P^\circ_{3/2}$	$+4\gamma,5\gamma$	$\rightarrow Kr^{2+}$	$4s^2 4p^4\,{}^3P_2+e^-$	1.08, 7.49		
c			$4\gamma,5\gamma$		${}^3P_1+e^-$	0.52, 6.93		
d			$4\gamma,5\gamma$		${}^3P_0+e^-$	0.43, 6.84		
e			5γ	$\rightarrow Kr^{2+}$	$4s^2 4p^4\,{}^1D_2+e^-$	5.67		
f			5γ		${}^1S_0+e^-$	3.38		
g	Kr^{2+}	$4s^2 4p^4\,{}^3P_2$	$+6\gamma,7\gamma$	$\rightarrow Kr^{3+}$	$4s^2 4p^3\,{}^4S^\circ_{3/2}+e^-$	1.57, 7.98		
h		${}^3P_1$	$+6\gamma,7\gamma$		$+e^-$	1.01, 7.42		
i		${}^3P_0$	$+6\gamma,7\gamma$		$+e^-$	0.92, 7.33		
j		${}^1D_2$	$+6\gamma,7\gamma$		$+e^-$	6.16,12.57		
k		${}^1S_0$	$+6\gamma,7\gamma$		$+e^-$	3.88,10.29		
					Argon			
a	Ar	$3s^2 3p^6\,{}^1S_0$	$+3\gamma,4\gamma,5\gamma,6\gamma,7\gamma$	$\rightarrow Ar^{1+}$	$3s^2 3p^5\,{}^2P^\circ_{3/2}+e^-$	3.48, 9.89,16.30,22.71,29.12		
b	Ar^{1+}	$3s^2 3p^5\,{}^2P^\circ_{3/2}$	$+5\gamma,6\gamma,7\gamma$	$\rightarrow Ar^{2+}$	$3s^2 3p^4\,{}^3P_2+e^-$	4.44,10.85,17.26		
c			$5\gamma,6\gamma,7\gamma$		${}^3P_1+e^-$	4.30,10.71,17.12		
d			$5\gamma,6\gamma,7\gamma$		${}^3P_0+e^-$	4.25,10.66,17.07		
e			$5\gamma,6\gamma,7\gamma$		${}^1D_2+e^-$	2.70, 9.11,15.52		
f			$5\gamma,6\gamma,7\gamma$		${}^1S_0+e^-$	0.31, 6.72,13.13		

ed by helium, argon, and krypton. As Table II shows, the electron contributions arising from the formation of higher charged ions is considerably less for argon and krypton at intensities below $\sim 10^{15}$ W/cm^2 than they are for xenon. In addition, for krypton the experimental situation is aggravated by the fact that the low-energy electron continuum between ~ 0 and 2 eV generated by scattered radiation may obscure all weak line features in this range. Furthermore, the krypton pressure has to be kept below $\sim 2\times 10^{-7}$ Torr in order to avoid detector saturation caused by the dominant 5.24-eV line shown in Fig. 3(b), an effect which will mask any lower-energy features.

The sequential ionization of the Kr^+ $2P^\circ_{3/2}$ ground state to the ground and low-lying excited Kr^{2+}-ion states

TABLE IV. Relative line intensities in the xenon electron-energy spectrum at a peak 193-nm intensity of 10^{15} W/cm^2. The line designations indicated correspond to the codes for the ionization channels (IC) given in Table III for xenon. The number associated with the code letter equals the number of photons absorbed in that channel and is in accord with the markings in Fig. 5. The intensities are normalized to line (b3,g4). The approximate relative ATI intensities for five-, six-, seven-, and eight-photon absorption are given in the right column. With the exception of the (a) and (b,g) series, these values are nearly independent of the ionization channel. The approximate relative channel intensities c, (d,e), f are shown in the bottom row for the fifth, sixth, and seventh order. These magnitudes are seen to be nearly independent of the order.

IC intensity		IC intensity		IC intensity		IC intensity		IC intensity		Relative ATI intensity
a2	(60)	b3,g4	100	c4	65	d,e4	(50)	f4	(35)	
a3	15–20	b4,g5	3	c5	13	d,e5	11	f5	48	100
a4	0.6	b5,g6	0.5	c6	2.7	d,e6	2.4	f6	9	20
a5	<0.01			c7	0.3	d,e7	0.2	f7	1	2
								f8	0.2	0.4
Approximate relative channel intensities for five-, six-, seven-photon absorption					29		25		100	

produces electron lines grouped around 0.9–1 eV for four-photon absorption (Table III) and around 6.8–7.5 eV for five-photon absorption. The lowest-order channels close at intensities in the range of 1.5×10^{14}–3×10^{14} W/cm^2. A careful study of many electron spectra recorded under different experimental conditions revealed that the feature observed in the krypton spectrum shown in Fig. 3(b) between 6.5 and 8.5 eV can be associated with these five-photon processes.

In Ar the sequential Ar^{2+} formation leads to electron lines around 4.3 eV (Table III). The inset illustrated in the argon spectrum of Fig. 3(c) which was recorded at a higher-energy resolution, clearly shows the expected feature, but slightly upshifted at around 5 eV. In addition, on the low-energy side of the structured peak occurring at ~10 eV, another line is seen which corresponds to six-photon ionization of Ar^+ $^2P^o_{3/2}$ with the final Ar^{2+} ion in the excited $^1D_2$ level (Table III). The combined intensity of these lines, relative to the neutral Ar ladder sequence, approximately reflects the measured relative abundances of the Ar^+ and Ar^{2+} ions listed in Table II.

In the helium spectrum, Fig. 3(e), the prominent ATI ladder from the first ionization step to the He^+ ground state is accompanied by a much weaker ATI ladder originating from the sequential removal of the second electron after absorption of nine and more photons and accounting for about 2% of all electrons detected in sharp lines.

If the direct process is important for argon, krypton, and helium, and if a substantial fraction of the electrons produced comprise a relatively low-energy continuum, then the experimental difficulties noted above interfere with their detection. Also, we recall, from the discussion in Sec. III A, that the probability for direct multiphoton absorption above the second ionization threshold must be quite low under the given experimental conditions.

4. Multiphoton inner-shell excitation. In addition to the photoionization of outer-shell electrons, highly-charged ions can be a final result arising from the initial formation of an inner-shell vacancy followed by electron rearrangement with the emission of radiation and Auger electrons in a cascade process.[63–67] The Auger spectra of the rare gases have been measured using both single-photon and electron impact ionization.[68–75] In multiphoton experiments inner-shell excitation is possible, in principle, either by direct high-order multiphoton coupling to the inner electron or by energy transfer from multiply excited outer-shell configurations. For the latter, it has been possible to formulate a model describing a possible mode of intrashell coupling by drawing an analogy with fast ion-atom and atom-atom collisions.[19,20] The known properties of free atoms suggest that this kind of coupling could be quite strong, particularly in certain regions of the periodic table.[4] In Xe, for example, the $5p$, $5s$, and $4d$ shells exhibit substantial intrashell coupling and behave in a collective fashion like a single super shell.[66,76–78] Direct inner-shell photoexcitation by the ultraviolet radiation is expected to be unlikely because of the screening[79] provided by the outer shells, an effect which is significant because the single-photon energy is below the outer-shell excitation energy.[80] However, at very high laser intensities, the strong intershell coupling is expected to cause a nonlinear response of the outer-shell electrons to the laser field and, consequently, the generation of higher harmonics of the field, which can then penetrate to inner shells and cause their ionization.[20,81]

Independent of the mechanism of excitation, the Auger decay of an inner-shell vacancy should result in an electron-energy spectrum with a characteristic pattern of lines. The spectrum consists of the principal decay line, leaving the doubly charged ion in the ground state, and an array of satellite lines caused by electron correlation[76,77] (shake-up) which leads to ion formation in an excited state.

In xenon, the energies of the $4s^95s^25p^6\,^2D_{5/2,3/2}$ $4d$-hole states are known[73,82] to be at 67.55 and 69.52 eV, respectively. The corresponding energies for the krypton $3d$-hole states $3d^94s^24p^6\,^2D_{5/2,3/2}$ are measured[82] to be at 93.82 and 95.04 eV, respectively. The strongest decay lines in the $N_{4,5}OO$ Auger spectrum of xenon are grouped around 35 eV with observed[73,75] low-energy satellites extending down to ~8 eV. In the $M_{4,5}NN$ Auger spectrum of krypton, the corresponding lines[74] are grouped around 55 eV with satellites of significant strength down to 25

eV. However, a close examination of our electron spectrum for xenon for intensities below 10^{15} W/cm^2, although revealing several prominent lines in the 8—22-eV region with spacings matching[83,84] the known[73] $4d_{5/2}$-$4d_{3/2}$ fine-structure splitting of 2 eV, does not give evidence for the expected features in the $\sim$35-eV range. At the same time, as described in Sec. III A and shown in Table III (for Xe) and Fig. 5, the main features of the observed electron spectra for xenon at intensities below $\sim 10^{15}$ W/cm^2 can be understood as arising from ATI ladder sequences involving the formation of Xe^+, Xe^{2+}, and Xe^{3+} with allowance made for the production of certain identified excited ionic states. Experimentally, the accidental coincidence, for 193-nm radiation, of certain ATI lines with the energies characteristic of the low-energy satellites of the xenon to $4d$ Auger decay prevents isolation of any Auger features even if present in the data. On the other hand, an inner-shell vacancy produced in a nonlinear process would undergo an Auger decay with a rate on the order of 10^{14} s^{-1} and electron energies characteristic of the charge state involved.[85] Since an atom responding in this way would be strongly perturbed by the intense ambient electromagnetic field, considerable energy shifts,[86] variations in the level widths, and changes of the branching ratios for Auger transitions are expected. In this connection it is interesting to recall that, in preliminary experiments[4] conducted at 193-nm intensities in the 10^{16}-W/cm^2 range, evidence was found for the production of energetic radiation (10 eV $\leq \hbar\omega \leq$ 80 eV) emitted by xenon with irradiation under collision-free conditions. Radiation of this energy could be produced by inner-shell transitions[67] or the emission of fluorescence following the multiphoton excitation of a near resonance in the outer shell of a xenon ion. However, since no evidence for such a process has been found in the electron spectra, the probability for this process at intensities below $\sim 10^{15}$ W/cm^2 must be fairly low unless the process of autoionization is suppressed or energetically forbidden.

C. Competition between direct and sequential processes

The present results on electron spectra indicate that the process of sequential ionization, modified by the presence of ATI, dominates the production of the electrons observed. However, it has also been indicated[19,20] that a direct mechanism of interaction, capable of producing both multiple ionization and inner-shell excitation,[84] could occur if certain motions of the atomic outer-shell electrons can be driven by the incident electromagnetic field. In the competition of these two mechanisms,[87] we now examine the nature of the conditions necessary for the enhancement of the direct process.

In order to maximize the probability for energy transfer between multiply excited configurations of outer-shell electrons and those occupying inner-shell orbits, the decay rate of the outer-shell excitation by electron emission must be sufficiently low[50] to permit the overall act of multiquantum absorption, involving both the excitation of outer electrons by the radiation field and the intershell energy transfer, to occur. Specifically, we want the escape of electrons from the vicinity of the atomic potential to be retarded. A possible means to achieve this is through the presence of the ponderomotive potential [of Eq. (8)]

$$U(I,\omega,t)=\frac{e^2\mathbf{E}_0^2(t)}{4m\omega^2}\ , \tag{12}$$

provided that its strength can be developed with sufficient rapidity to effectively discourage electron emission into the available channels. In expression (12) the explicit dependencies on laser intensity I through the field strength $\mathbf{E}_0$, frequency ω, and time t have been indicated. One possible statement of the condition necessary is that the ponderomotive potential $U(I,\omega,t)$ increases an amount equal to the quantum energy ($\hbar\omega$) in the time scale τ_e characterizing electron emission during the course of irradiation. In this situation, the atomic electrons experience a sequence of closing channels at successively higher energies as radiation is absorbed by the atom. This statement can be written as

$$\frac{\partial U(I,\omega,t)}{\partial t}=\frac{\hbar\omega}{\tau_e}\ . \tag{13}$$

Since the ponderomotive potential [cf. Eq. (8)] can be written as

$$U(I,\omega,t)=\left[\frac{2\pi e^2}{mc\omega^2}\right]I(t)\ , \tag{14}$$

the result

$$\frac{dI(t)}{dt}=\frac{mc\hbar\omega^3}{2\pi e^2\tau_e} \tag{15}$$

follows. If, for simplicity, we consider a triangular pulse with a maximum intensity I_0 which rises linearly in time over a period τ, Eq. (15) for the theoretically required condition can be put in the form

$$\frac{I_0}{\tau}=\beta\equiv\frac{mc\hbar\omega^3}{2\pi e^2\tau_e}\ , \tag{16}$$

or equivalently,

$$\tau=\tau_e\left[\frac{2\pi e^2 I_0}{mc\hbar\omega^3}\right]=(2\pi\alpha)\tau_e\left[\frac{I_0}{I_\omega}\right] \tag{17}$$

with

$$I_\omega\equiv m\omega^3 \tag{18}$$

and α denoting the fine-structure constant. In expression (17), for the time scale τ necessary, two parameters occur. One characterizes the maximum intensity I_0, a factor under experimental control, while the other is the electron emission time τ_e, viewed in this simple picture as an intrinsic atomic parameter. It may be, of course, that τ_e is influenced by the instantaneous intensity and the order N of the process, but these complications are not considered here.

An approximate value for the time scale τ_e can be related to the data on the electron spectra shown in Table III, Fig. 3, and Fig. 5. We observe that, although ionic excited states are evident, no levels with excited configurations are present. Specifically, no state representing a configu-

TABLE V. Compilation of the parameters of several extant studies of collision-free nonlinear processes. The wavelength of irradiation is denoted by λ, I_{expt} is the peak experimental intensity, τ_p is the experimental pulse width, I_ω is defined by Eq. (18), $\gamma \equiv I_{\text{expt}}/\tau_p$, $\beta \equiv mc\hbar\omega^3/2\pi e^2\tau_e$ with $\tau_e = 10^{-15}$ s, and $U(I_{\text{expt}},\omega)$ is the ponderomotive potential. Reference numbers are also listed.

λ (μm)	I_{expt} (W/cm^2)	τ_p (fs)	I_ω (W/cm^2)	γ $\left[\frac{\text{W}}{\text{cm}^2\,\text{s}}\right]$	β $\left[\frac{\text{W}}{\text{cm}^2\,\text{s}}\right]$	β/γ	$U(I_{\text{expt}},\omega)$ (eV)	Ref.
0.193	$\sim 10^{15}$	$\sim 5\times 10^3$	8.3×10^{13}	2×10^{26}	1.8×10^{30}	9.1×10^3	~ 3.84	This work
0.355	$\sim 10^{13}$	$\sim 10^4$	1.3×10^{13}	10^{24}	2.8×10^{29}	2.8×10^5	~ 0.12	13
0.53	$\sim 10^{13}$	$\sim 10^4$	4.0×10^{12}	10^{24}	8.7×10^{28}	8.7×10^4	~ 0.26	13
0.53	$\sim 10^{12}$	$\sim 5\times 10^3$ $\sim 2\times 10^5$	4×10^{12}	5×10^{21} 2×10^{23}	8.7×10^{28}	4.3×10^5 1.7×10^7	~ 0.03	62,87
1.06	$\sim 4\times 10^{16}$	$\sim 2.5\times 10^4$	5×10^{11}	1.6×10^{27}	1.1×10^{28}	6.9	~ 4190	8,17
1.06	$\sim 10^{13}$	$\sim 10^4$	5×10^{11}	10^{24}	1.1×10^{28}	1.1×10^4	~ 1.05	13
1.06	$\sim 10^{11}$–10^{13}	$\sim 5\times 10^4$	5×10^{11}	2×10^{21} 2×10^{23}	1.1×10^{28}	5.5×10^4 5.5×10^6	~ 0.01–1.0	16
1.06	$\sim 10^{13}$	$\sim 5\times 10^3$ $\sim 2\times 10^5$	5×10^{11}	5×10^{22} 2×10^{24}	1.1×10^{28}	5.5×10^3 2.2×10^5	~ 1.05	62,87
10.6	$\sim 10^{14}$	$\sim 1.1\times 10^6$	5×10^8	9.1×10^{22}	1.1×10^{25}	1.2×10^2	~ 1040	5

ration involving an excited (n,l) orbital is detected and, as discussed in Sec. III A, no influence of such excited states was seen on the intensity distributions of the observed electron spectra. This experimental fact suggests that the process of electron removal is, for the conditions studied, adiabatic with respect to the electronic orbital motion. Equivalently, shake-up arising from the electron emission is negligible. Since all the ionic species of xenon listed in Table III have states with excited configurations lying approximately[26] 10^5 cm^{-1} above their respective ionic ground states, the time τ_e should be long compared to $\sim 3.3\times 10^{-16}$ s in order to respect this condition for adiabaticity. Therefore, for the estimates furnished below in Table V, we will use the value $\tau_e \simeq 10^{-15}$ s.

Table V contains a compilation of the parameters for several extant studies of collision-free nonlinear processes and gives the characteristic ranges over which these experiments have been performed. The conditions of these studies can then be compared to the criterion stated in Eq. (13) by the introduction of a factor γ defined as

$$\gamma \equiv I_{\text{expt}}/\tau_p \ , \tag{19}$$

the experimental counterpart of the theoretically required condition stated in Eq. (16). The column (β/γ) then gives a direct measure of the departure of the experimental conditions from that expressed in Eq. (13). Specifically, values of $\beta/\gamma > 1$ indicate that the necessary conditions are not satisfied. The large values of β/γ shown in Table V demonstrate that most experiments conducted thus far fail to satisfy the conditions of Eq. (13) by a significant margin, by factors of a thousand or more. Therefore, within the framework of this type of physical picture, the sequential process would be expected to play the major, if not dominant role, in these experiments.[50] Finally, a comparison of the peak ponderomotive potential $U(I_{\text{expt}},\omega)$ appearing in Table V for the experiment of Baldwin and Boreham,[17] who observed a maximum electron energy of 400–500 eV, shows that the observed electron energy corresponds approximately to a value 1 order of magnitude lower than the peak ponderomotive potential. This correspondence gives an indication of the physical significance of the criterion estimated with Eq. (13).

We now inquire into the possibility of entering the regime of which $\beta/\gamma \leq 1$, the range of intensities and pulse widths which is in conformance with the general criterion of Eq. (13). On the basis of earlier estimates[4,19,20] it has been suggested that the direct process is favored if the atom is exposed to a radiative electric field E significantly greater than an atomic unit ($E_a = e/a_0^2$). An intensity $I_0 \simeq 10^{18}$ W/cm^2, a value corresponding to a few atomic units of electric field and believed to be technically feasible with modern light sources,[1(b)] would satisfy this condition. Therefore, we will use this intensity scale in order to estimate the maximum pulse width permissible for 248-nm radiation. At the wavelength of 248 nm, $I_\omega = 3.9\times 10^{13}$ W/cm^2, or equivalently, $\beta = 8.5\times 10^{29}$ W/cm^2 s. Consequently, $\beta/\gamma = 1$ implies that $\tau_p \simeq 1.2\times 10^{-12}$ s. Therefore, a KrF* (248-nm) source capable of $\sim$1-ps operation and focusable to $\sim 10^{18}$ W/cm^2 would enable experiments to be conducted under the appropriate physical conditions. Fortunately, the technical feasibility of such an instrument is manifest,[1(b)] so that studies in this interesting physical regime will be conducted in the near future. According to this analysis, with irradiation at 248 nm at a peak pulse intensity of $\sim 10^{18}$ W/cm^2, the electrons would be trapped in a ponderomotive potential with a depth of several keV.

IV. SUMMARY

The energy spectra of electrons generated by collision-free multiphoton ionization of Xe, Kr, Ar, Ne, and He exposed to picosecond 193-nm radiation have been studied up to an intensity of $\sim 10^{15}$ W/cm^2. In addition to the appearance of the lowest-order ionization lines, all spectra exhibit above-threshold ionization (ATI) transitions, although with considerably lower intensity. The probabilities of ionization and the branching into specific final ion states appear sensitive to the presence of near resonances with excited atomic states. The rapid decrease in the electron line intensity with increasing nonlinear order N of the process, in comparison to corresponding spectra ob-

tained at visible and infrared wavelengths, is qualitatively in agreement with calculations of the transition probability which take into account the temporal laser pulse shape and saturation. No shift of the measured electron spectral features could be unambiguously attributed to the dynamic Stark effect or the influence of the ponderomotive force. Furthermore, the influence of excited ionic configurations, multiply excited valence-shell levels, or inner-shell excited states on the observed intensity patterns of ATI lines appears to be negligible.

In the formation of higher-charged ions, the data indicate that the sequential liberation of electrons is the dominant process governing the interaction over the range of physical parameters studied. This characteristic of the process is most evident in the electron spectra exhibited by xenon. In this case, the appearance of overlapping ATI ladder series shows that the sequential mechanism is the main process leading to the formation of Xe^{2+} and Xe^{3+}.

The closing of specific low-energy channels due to the influence of the ponderomotive potential has also been observed and the intensities at which these channels are suppressed conform qualitatively to that predicted theoretically. It seems possible, that in properly conducted experiments, that this effect could be used to estimate the laser intensity in the focal volume in which most of the ionizing events occur.

An examination of the competition between mechanisms of direct multiple ionization and sequential ionization leads to the conclusion that, given the range of physical conditions studied, all experiments conducted so far are expected to favor ionization by the sequential process. Conversely, enhancement of the direct process may occur in a physical regime for which the emission of electrons in low-energy channels is sufficiently retarded by the influence of the ponderomotive potential. The conditions necessary to examine this situation can be experimentally realized by modern ultraviolet sources operating in the subpicosecond region.

The two-photon line for Xe, the lowest-order ionization process for that material at 193 nm, is located energetically adjacent to the autoionizing Rydberg series which converges to the $5s^2 5p^5\,^2P^{\circ}_{1/2}$ excited ion state. This feature is observed to split into a well-resolved doublet at laser intensities between 10^{10} and 10^{12} W/cm^2 and laser pulse lengths of ~ 10 ns. This observation has been tentatively interpreted as arising from the Autler-Townes effect.

Note added. Recently, stepwise multiphoton double ionization has also been directly observed in photoelectron spectra from strontium.[88] The upshift of the average photoelectron energy with laser intensity in multiphoton ionization of rare gases has been seen at longer wavelengths also.[89]

ACKNOWLEDGMENTS

The authors wish to acknowledge fruitful discussions with A. P. Schwarzenbach, I. A. McIntyre, A. McPherson, K. Boyer, and A. Szöke as well as the technical assistance of M. Scaggs, R. Slagle, and J. Wright. This work was supported by the U.S. Office of Naval Research, the U.S. Air Force Office of Scientific Research under Contract No. F49620-83-K0014, the Innovative Science and Technology Office of the Strategic Defense Initiative Organization, the U.S. Department of Energy under Grant No. DE-AC02-83ER13137, the Lawrence Livermore National Laboratory under Contract No. 5765705, the National Science Foundation under Grant No. PHY 84-14201, the U.S. Air Force Office of Scientific Research, Department of Defense University Research Instrumentation Program under Grant No. USAF 840289, the U.S. Defense Advanced Research Projects Agency, and the Los Alamos National Laboratory under Contract No. 9-X54-C6096-1.

*Present address: Lambda Physik, Hans-Böckler-Strasse 12, D-3400 Göttingen, Federal Republic of Germany.

[1]For reviews see: (a) *Multiphoton Ionization of Atoms,* edited by S. L. Chin and P. Lambropoulos, (Academic, New York, 1984); (b) C. K. Rhodes, Science **229**, 1345 (1985).

[2]A. L'Huillier, L. A. Lompré, G. Mainfray, and C. Manus, Phys. Rev. Lett. **48**, 1814 (1982); Phys. Rev. A **27**, 2503 (1983).

[3]T. S. Luk, H. Pummer, K. Boyer, M. Shahidi, H. Egger, and C. K. Rhodes, Phys. Rev. Lett. **51**, 110 (1983).

[4]T. S. Luk, U. Johann, H. Egger, H. Pummer, and C. K. Rhodes, Phys. Rev. A **32**, 214 (1985).

[5]S. L. Chin, F. Yergeau, and P. Lavigne, J. Phys. B **18**, L213 (1985).

[6]M. Hollis, Opt. Commun. **25**, 395 (1978).

[7]P. Agostini, F. Fabre, G. Mainfray, G. Petite, and N. K. Rahman, Phys. Rev. Lett. **42**, 1127 (1979).

[8]B. W. Boreham and B. Luther-Davis, J. Appl. Phys. **50**, 2533 (1979).

[9]P. Kruit, J. Kimman, and M. J. van der Wiel, J. Phys. B **14**, L597 (1981).

[10]K. Boyer, H. Egger, T. S. Luk, H. Pummer, and C. K. Rhodes, J. Opt. Soc. Am. B **1**, 3 (1984).

[11]G. Petite, F. Fabre, P. Agostini, M. Crance, and M. Aymar, Phys. Rev. A **29**, 2677 (1984).

[12]F. Fabre, G. Petite, P. Agostini, and M. Clement, J. Phys. B **15**, 1353 (1982).

[13]P. Kruit, J. Kimman, H. G. Muller, and M. J. van der Wiel, Phys. Rev. A **28**, 248 (1983).

[14]M. Gavrila, A. Maquet, and V. Véniard, Phys. Rev. A **32**, 2537 (1985).

[15]A. L'Huillier, L. A. Lompré, G. Mainfray, and C. Manus, J. Phys. B **16**, 1363 (1983).

[16]L. A. Lompré, A. L' Huillier, G. Mainfray, and J. Y. Fan, J. Phys. B **17**, L817 (1984).

[17]K. G. H. Baldwin and B. W. Boreham, J. Appl. Phys. **52**, 2627 (1981).

[18]C. K. Rhodes, *Fundamentals of Laser Interactions,* No. 229 of *Lecture Notes in Physics,* edited by F. Ehlotzky (Springer-Verlag, Berlin, 1985), p. 111.

[19]K. Boyer and C. K. Rhodes, Phys. Rev. Lett. **54**, 1490 (1985).

[20]A. Szöke and C. K. Rhodes, Phys. Rev. Lett. **56**, 720 (1986).

[21]H. Egger, T. S. Luk, K. Boyer, D. R. Muller, H. Pummer, T. Srinivasan, and C. K. Rhodes, Appl. Phys. Lett. **41**, 1032

(1982).
[22]T. Hsu and J. L. Hirshfield, Rev. Sci. Instrum. **47**, 236 (1976).
[23]G. Beamson, H. Q. Porter, and D. W. Turner, J. Phys. E **13**, 64 (1980).
[24]P. Kruit and F. H. Read, J. Phys. E **16**, 373 (1983).
[25]B. W. Boreham and H. Hora, Phys. Rev. Lett. **42**, 776 (1977).
[26]C. E. Moore, *Atomic Energy Levels,* Natl. Bur. Stand. Ref. Data Ser., Natl. Bur. Stand. (U.S.) Circ. No. 467 (U.S. GPO, Washington, D.C., 1971), Volumes I–III.
[27]S. L. Chin and N. R. Isenor, Can. J. Phys. **48**, 1446 (1970).
[28]L. V. Keldysh, Zh. Eksp. Teor. Fiz. **47**, 7 (1964) [Sov. Phys.—JETP **20**, 4 (1965)].
[29]Yu. P. Raizer, Usp. Fiz. Nauk **87**, 29 (1965) [Sov. Phys.—Usp. **8**, 650 (1966)].
[30]W. K. Bischel, J. Bokor, D. J. Kligler, and C. K. Rhodes, IEEE J. Quantum Electron. **QE-15**, 380 (1979); J. Bokor, J. Zavelovich, and C. K. Rhodes, Phys. Rev. A **21**, 1453 (1980).
[31]L. A. Lompré, G. Mainfray, C. Manus, and J. Trebault, J. Phys. **39**, 610 (1978); T. Srivasan, H. Egger, T. S. Luk, H. Pummer, and C. K. Rhodes, IEEE J. Quantum Electron. **QE-19**, 1874 (1983).
[32]N. B. Delone and V. P. Krainov, *Atoms in Strong Light Fields,* Vol. 28 of *Springer Series in Chemical Physics,* edited by F. P. Schäfer (Springer-Verlag, Berlin, 1985).
[33]R. F. Stebbings, F. B. Dunning, and R. D. Pundel, in *Atomic Physics 4,* edited by G. zu Putlitz, E. W. Weber, and A. Winnacher (Plenum, New York, 1975), p. 713.
[34]F. J. Wuilleumier, M. Y. Adam, P. Ihez, N. Sandner, V. Schmitz, and W. Mehlhorn, Phys. Rev. A **16**, 646 (1977).
[35]R. N. Compton, J. C. Miller, A. E. Carter, and P. Kruit, Chem. Phys. Lett. **71**, 87 (1980).
[36]Shih-I Chu and J. Cooper, Phys. Rev. A **32**, 2769 (1985).
[37]M. Crance and M. Aymar, J. Phys. B **13**, L421 (1980).
[38]Y. Gontier and M. Trahin, J. Phys. B **13**, 4383 (1980).
[39]T. P. Hughes, *Plasmas and Laser Light* (Wiley, New York, 1975).
[40]M. Crance, J. Phys. B **17**, L355 (1984).
[41]M. Crance, J. Phys. B **17**, L155 (1984).
[42]H. Egger, U. Johann, T. S. Luk, and C. K. Rhodes, J. Opt. Soc. Am. (to be published).
[43]R. P. Madden, D. L. Ederer, and K. Codling, Phys. Rev. **177**, 136 (1969).
[44]K. Codling and R. P. Madden, Phys. Rev. **4**, 2261 (1971).
[45]R. W. Carman, private communication.
[46]J. A. Baxter, P. Mitchell, and J. Comer, J. Phys. B **15**, 1105 (1982).
[47]T. Srinivasan, W. Müller, M. Shahidi, T. S. Luk, H. Egger, H. Pummer, and C. K. Rhodes, J. Opt. Soc. Am. B (to be published).
[48]T. Srinivasan, H. Egger, T. S. Luk, H. Pummer, and C. K. Rhodes, in *Laser Spectroscopy VI,* edited by H. P. Weber and W. Lüthy (Springer-Verlag, Berlin, 1983), p. 385; K. Boyer, H. Egger, T. S. Luk, H. Pummer, and C. K. Rhodes, J. Opt. Soc. Am. B **1**, 3 (1984).
[49]C. K. Rhodes, in *Multiphoton Processes,* edited by P. Lambropoulos and S. J. Smith (Springer-Verlag, Berlin, 1984), p. 31; L. A. Lompré and G. Mainfray, *ibid.*, p. 23; D. Feldman, H.-J. Krautwald, and K. H. Welge, in *Multiphoton Ionization of Atoms,* edited by S. L. Chin and P. Lambropoulos (Academic, New York, 1984), p. 223; W. B. Delone, V. V. Suran, and B. A. Zon, *ibid.*, p. 235.
[50]P. Lambropoulos, Phys. Rev. Lett. **55**, 2141 (1985).
[51]H. G. Muller, A. Tip, and M. J. van der Wiel, J. Phys. B **16**, L679 (1983).
[52]H. G. Muller and A. Tip, Phys. Rev. A **30**, 3039 (1984).
[53]M. Edwards, L. Pan, and L. Armstrong, Jr., J. Phys. B **17**, L515 (1984).
[54]Z. Bialynicka-Birula, J. Phys. B **17**, 2097 (1984).
[55]M. H. Mittleman, Phys. Rev. A **29**, 2245 (1984).
[56]A. Szöke, J. Phys. B **18**, L427 (1985).
[57]T. S. B. Kibble, Phys. Rev. A **150**, 1060 (1966).
[58]E. J. McGuire, Phys. Rev. A **24**, 835 (1981).
[59]S. H. Autler and C. H. Townes, Phys. Rev. **100**, 703 (1955).
[60]K. Rzażewski and J. H. Eberly, Phys. Rev. A **27**, 2026 (1983).
[61]U. Fano, Phys. Rev. **124**, 1866 (1961).
[62]A. L'Huillier, L. A. Lompré, G. Mainfray, and C. Manus, J. Phys. (Paris) **44**, 1247 (1983).
[63]T. A. Carlson, W. E. Hunt, and M. O. Krause, Phys. Rev. **151**, 41 (1966),
[64]M. O. Krause and T. A. Carlson, Phys. Rev. **158**, 18 (1967).
[65]J. Berkowitz, *Photoabsorption, Photoionization and Photoelectron Spectroscopy* (Academic, New York, 1979).
[66]M. J. van der Wiel and T. N. Chang, J. Phys. B **11**, L125 (1978).
[67]H. Hertz, Z. Phys. **274**, 289 (1975).
[68]W. Mehlhorn, W. Schmitz, and D. Stalherm, Z. Phys. **252**, 399 (1972).
[69]L. O. Werme, T. Bergmark, and K. Siegbahn, Phys. Scr. **8**, 149 (1973).
[70]L. O. Werme, T. Bergmark, and K. Siegbahn, Phys. Scr. **6**, 141 (1972).
[71]S. Ohtani, H. Nishimura, H. Suzuki, and K. Wakiya, Phys. Rev. Lett. **36**, 863 (1976).
[72]W. Eberhardt, G. Kalkoffen, and C. Kunz, Phys. Rev. Lett. **41**, 156 (1978).
[73]S. Southworth, U. Becker, and C. M. Truesdale, P. H. Kobrin, D. W. Lindle, S. Owaki, and D. A. Shirley, Phys. Rev. A **28**, 261 (1983).
[74]H. Aksela, S. Aksela, and H. Pulkkinin, Phys. Rev. A **30**, 2456 (1984).
[75]H. Aksela, S. Aksela, and H. Pulkkinin, Phys. Rev. A **30**, 865 (1984).
[76]M. Ya. Amusia, in *Advances in Atomic and Molecular Physics,* edited by D. R. Bates and B. Bederson (Academic, New York, 1981), Vol. 17, p. 1.
[77]G. Wendin, *Breakdown of the One-Electron Picture in Photoelectron Spectra,* Vol. 45 of *Structure and Bonding* (Springer-Verlag, Berlin, 1981).
[78]G. Wendin, Comments At. Mol. Phys. **17**, 115 (1986).
[79]A. Zangwill and P. Soven, Phys. Rev. Lett. **45**, 204 (1980); A. Zangwill and P. Soven, Phys. Rev. A **21**, 1561 (1980).
[80]G. Wendin, L. Jönsson, and A. L.' Huillier, Phys. Rev. Lett. **56**, 1241 (1986).
[81]A. Zangwill, J. Chem. Phys. **78**, 5926 (1983).
[82]K. Codling and R. P. Madden, Phys. Rev. Lett. **12**, 106 (1964).
[83]U. Johann, T. S. Luk, H. Egger, H. Pummer, and C. K. Rhodes, in Technical Digest, Conference on Lasers and Electro-Optics '85, Baltimore, Maryland (unpublished), p. 152.
[84]U. Johann, T. S. Luk, and C. K. Rhodes, *Fourteenth International Conference on the Physics of Electronic and Atomic Collisions,* edited by D. C. Lorents, W. E. Meyerhof, and J. R. Peterson (North-Holland, Amsterdam, 1985).
[85]D. C. Griffin, C. Bottcher, M. S. Pindzola, S. M. Younger, D. C. Gregory, and D. C. Crandall, Phys. Rev. A **29**, 1720 (1984).
[86]F. P. Larkins, J. Phys. B **6**, 2450 (1973).

[87]L. Lompré and G. Mainfray, in *Fundamentals of Laser Interactions,* No. 229 of *Lecture Notes in Physics,* edited by F. Ehlotzky (Springer-Verlag, Berlin, 1985), p. 125.

[88]P. Agostini and G. Petite, Phys. Rev. A **32**, 3800 (1985).

[89]L. A. Lompré, A. L'Huillier, G. Mainfray, and C. Manus, J. Opt. Soc. Am. B **2**, 1906 (1985).